SMRT | A WORLD OF KNOWLEDGE
FOR MR TECHNOLOGISTS & RADIOGRAPHERS

SECTION FOR MAGNETIC RESONANCE TECHNOLOGISTS
OF THE INTERNATIONAL SOCIETY FOR MAGNETIC RESONANCE IN MEDICINE

Home Studies Educational Seminars

VOLUME 14 • NUMBER 3

MR Imaging Physics Tutorial



AAPM/RSNA Physics Tutorial for Residents Fundamental Physics of MR Imaging

Robert A. Pooley, Ph.D.

AAPM/RSNA Physics Tutorial for Residents MR Imaging: Brief Overview and Emerging Applications

Michael A. Jacobs, Ph.D.
Tamer S. Ibrahim, Ph.D.
Ronald Ouwerkerk, Ph.D.

Expert Reviewer:
Chesanie E. Beam, B.S., R.T.(R)(M)(MR)

SMRT Educational Seminars Editor:
Anne Marie Sawyer, B.S., R.T. (R)(MR), FSMRT

The Section for Magnetic Resonance Technologists would like to thank Invivo for its generous support of this SMRT Educational Seminar.



*CAUTION!

Whether it's for prostate or breast, having both ***MRI analysis*** *and* ***MRI interventional capabilities*** *together, may cause people to react with extreme excitement!*



DynaTRIM



Luminescence BREAST SYSTEM

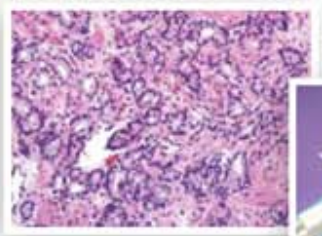
DynaCAD for PROSTATE

Leave it to Invivo to be the first with a complete clinical solution to visualize and target, under MRI-guidance, specific suspicious areas in the prostate.

A powerful MRI analysis system to:

- Quickly process and manage large volumes of images, opening ready to read
- Automated, computer-guided interventions with DynaTRIM

DynaTRIM (Trans-Rectal Interventional MRI) for targeted biopsies of the prostate may be an alternative solution for patients with rising PSA levels and negative TRUS biopsies.





MEDICAL DESIGN EXCELLENCE AWARDS® 2010 WINNER

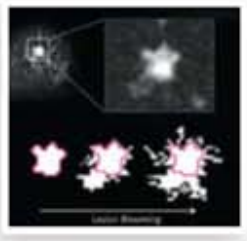
DynaCAD with ONCAD

shaping the diagnosis

We know what you are up against. The time it takes to go through your images can be long and difficult. This is why we strive to find better ways to assist you.

Our new DynaCAD with ONCAD delivers improved workflow with clinically tested morphological analysis. Only ONCAD automatically analyzes the entire dataset and draws attention to suspicious morphology.

- Finds suspicious lessions on MR, based on Morphology
- Adds confidence with "Second Check"
- Automatically displays results on DynaCAD
- Improves Workflow



Invivo

inspired by a better way

invivocorp.com

SMRT ELECTRONIC-ONLY & VIDEO HOME STUDIES

By Editor, Anne Marie Sawyer, B.S., R.T.(R)(MR), FSMRT

For the past thirteen years, the SMRT home studies have provided our members with a convenient way to obtain continuing education (CE) credits. Quarterly issues containing several articles provide credits awarded through the completion of a quiz that accompanies each home study. The accreditation is conducted by the SMRT acting as a RCEEM (Recognized Continuing Education Evaluation Mechanism) for the ARRT. Category A credits are assigned to each home study, which can be used to maintain one's ARRT advanced registry and are approved for AIR (Australian Institute of Radiography) continuing professional development (CPD) activities. SMRT members located in other countries who are interested in investigating the possibility of having our home studies, printed or electronic, approved for continuing education or professional development should contact Jennifer Olson, Associate Executive Director of the ISMRM/SMRT in Berkeley, California, USA at jennifer@ismrm.org for additional information.

The home study articles, selected by members of the SMRT publications committee, are obtained from peer-reviewed journals or written specifically for our publication by technologists, scientists or clinicians working in the field of magnetic resonance imaging (MRI). The quiz is written and expertly reviewed by members of the publication committee, volunteers from the SMRT and ISMRM membership or selected clinicians and scientists. The topics have included a variety of interests from basic physics and principles to clinical applications and anatomy and physiology atlases. Recent issues are available to members in both printed and electronic format.

As a method to provide an increased number of CE credits to the membership without increasing costs, electronic-only home studies and video home studies are now available through the SMRT website. As a means to minimize costs and to focus on becoming more environmentally conscious, SMRT members will see an increase in electronic-only and video home studies and a reduction in the number of pages in our printed publication.

Please visit the SMRT home study website at: http://www.ismrm.org/smrt/home-studies/. The SMRT will continue to add new electronic-only and video home studies in the near future.

Electronic Home Studies		
Title	**Category A CE & CPD Credits**	**Date**
Safety of MRI in Patients with Cardiovascular Devices	1	September 2008
Use of Contrast Agents in MR Imaging of the Spine	1	January 2009
Techniques in Spine MR Imaging	1	June 2010
Susceptibility-Weighted MR Imaging (SWI)	1	November 2010
Video Home Studies		
Cardiac MRI Forum	2	May 2011
MR Safety Forum	2	May 2011
Emerging Technologies Forum	1	May 2011



Anne Marie Sawyer, B.S., R.T.(R)(MR), FSMRT
Editor, SMRT Educational Seminars
Home Study Program
Lucas Center for Imaging
Stanford University, Stanford, California, USA
T: +1 650 725 9697 • E: amsawyer@stanford.edu



John J. Totman, DCR(R), M.Sc.
Chair, SMRT Publications Committee
Medical Physics & Clinical Engineering
Nottingham University Hospitals
Nottingham, UK
E: jjtotman@gmail.com

MR Imaging Physics Tutorial

October 2011

We are pleased to present the SMRT Educational Seminars, Volume 14, Number 3: "MR Imaging Physics Tutorial." This is the 53rd accredited home study developed by the SMRT, exclusively for the SMRT members. The accreditation is conducted by the SMRT acting as a RCEEM (Recognized Continuing Education Evaluation Mechanism) for the ARRT. Category A credits are assigned to each home study, which can be used to maintain one's ARRT advanced registry and are approved for AIR (Australian Institute of Radiography) continuing professional development (CPD) activities.

With the multitude of emerging applications in MR imaging, one must wonder, "Why a basic review of MR physics now?" As with most medical imaging, possessing a working knowledge of the fundamental building blocks is what allows us to move forward and more easily embrace, understand and effectively apply newer, more complex techniques. In addition, it is an opportunity to engage and teach technologists and radiographers new to the field of MR imaging. Finally, it never ceases to amaze this technologist of how fortunate we are to work in a field that is just pure magic as it continues to encourage the development of new ideas and applications. Looking to be challenged on a daily basis? Of course we are.

"Why a basic review of MR physics now?" As with most medical imaging, possessing a working knowledge of the fundamental building blocks is what allows us to move forward and more easily embrace, understand and effectively apply newer, more complex techniques."

Two articles have been selected for this SMRT home study, both originally written by Ph.D.s for M.D.s. Is it complex? Of course it is. Is it understandable by technologists and radiographers? Of course it is. It is important to remember that not all MR physics articles are created equal. Each one has its own specific twist on MR imaging. Therefore, we must read many to ensure we not only discover the truth but we find those that help us understand the most complex details. As we are all unique individuals, so are the ways we learn and retain information.

In the article Fundamental Physics of MR Imaging, the authors state, "For radiologists who interpret magnetic resonance (MR) images, it is extremely important to understand the mechanisms that are used to create the image data." While I agree it is important for radiologists to understand the physics and principles of MR imaging, it is equally important for the technologists and radiographers to do so as well. For it is we who sit at the controls and ensure optimum image quality is produced in the MRI scans. A very wise radiologist once told this technologist (albeit very young at the time), "I am only as good as the images you generate." At the time that happened to be x-rays but it has remained true for all imaging modalities.

"MR imaging plays an increasingly important role in radiologic imaging of different pathologic disorders, where the goal is developing radiologic imaging markers for noninvasive prediction of disease and response to treatment." This is a heads-up for us from the authors of the second article regarding the significant role that we as technologists and radiographers will play in the monumental changes coming our way in the advancement of health care.

Many thanks to Chesanie E. Beam, B.S., R.T.(R)(M)(MR) from Gastoria, North Carolina, USA, for acting as our Expert Reviewer for this home study issue and the accompanying quiz that provides the continuing education credits.

Thanks to John Totman, SMRT Publications Chair from Nottingham, UK, for directing and supporting the home studies program. Thanks also to Jennifer Olson, Associate Executive Director, Mary Keydash, Publications Director, and the staff in the Berkeley, California, USA office of the ISMRM/SMRT for their insight and long hours supporting these educational symposia.

We would especially like to thank John Wilkie and all of the people at Invivo Corporation (Philips Healthcare) who generously support our home studies program, the SMRT Educational Seminars. Their continuing investment advancing technologist and radiographer knowledge brings quality continuing education to the SMRT membership worldwide.

SECTION FOR MAGNETIC RESONANCE TECHNOLOGISTS

Home Studies Educational Seminars

VOLUME 14 • NUMBER 3

Educational Objectives

Fundamental Physics of MR Imaging

- Review the basic concepts including resonance and precession.
- Describe radiofrequency energy, its absorption and the role it plays in MRI.
- Discuss T1 and T2 relaxation and contrast including diagrams and image examples.
- Explain the components of spin echo MR imaging using pulse sequence diagrams.
- Review the effects of TE and TR and the resulting contrast formation.
- Describe the variations of spin echo MR imaging including multiecho, turbo, and inversion recovery.
- Introduce gradient echo MR imaging.

MR Imaging: Brief Overview and Emerging Applications

- Describe MR instrumentation including magnet designs, field strength, and shim, gradient, and RF coils.
- Explain the process of MR signal localization used in image reconstruction.
- Review gradients and their application used in localization including slice-selection, frequency- and phase-encoding.
- Discuss MR signal in the form of T1 and T2.
- Introduce k-space and its formation and effect on MR images generated.
- Describe parallel imaging and the initial variations.
- Discuss specific applications, basic and advanced, including diffusion-weighted imaging and spectroscopy.

Expert Reviewer



Chesanie E. Beam, B.S.,R.T.(R)(M)(MR)
Caromont Imaging Services
Gastoria, North Carolina, USA

NZIMRT APPROVED CPD ACTIVITY
SMRT Home Studies
1 Credit per study to a maximum of 10 per year
Valid to 31-12-2011

AIR Approved CPD Activity
2011 SMRT Educational Seminars Home Studies
credit levels according to SMRT certificate
Appellation 389.2 Valid to 31st December 2011

AAPM/RSNA Physics Tutorial for Residents

Fundamental Physics of MR Imaging[1]

Robert A. Pooley, Ph.D.

Reprinted with permission from Radiological Society of North America, Radiographics 2005, Volume 25, Pages 1087 - 1099, © RSNA, 2005

Learning the basic concepts required to understand magnetic resonance (MR) imaging is a straightforward process. Although the individual concepts are simple, there are many concepts to learn and retain simultaneously; this situation may give the illusion that learning the physics of MR imaging is complicated. It is important for the radiologist who interprets MR images to understand the methods used to create the images because image contrast specifically depends on how the image data were acquired. Initial concepts include formation of magnetic fields from electric currents in loops of wire, the resonance phenomenon, the hydrogen proton and its frequency of precession, and absorption of radiofrequency energy. These concepts can then be applied to learn about T1 and T2 relaxation and contrast and how the acquisition parameters of echo time and repetition time can be used to achieve these image contrasts. Basic pulse sequences include the spin-echo, multiecho spin-echo, turbo spin-echo, inversion-recovery, and gradient-recalled-echo sequences.

©RSNA, 2005

Abbreviations: ADC = analog-to-digital converter, CSF = cerebrospinal fluid, RF = radiofrequency, TE = echo time, TR = repetition time

RadioGraphics 2005; 25:1087–1099 • **Published online** 10.1148/rg.254055027 • **Content Codes:** MR PH

[1]From the Department of Radiology, Mayo Clinic, 4500 San Pablo Rd, Jacksonville, FL 32224. From the AAPM/RSNA Physics Tutorial at the 2004 RSNA Annual Meeting. Received February 11, 2005; revision requested March 22 and received April 22; accepted April 25. The author has no financial relationships to disclose. **Address correspondence to** the author (e-mail: *pooley.robert@mayo.edu*).

©RSNA, 2005

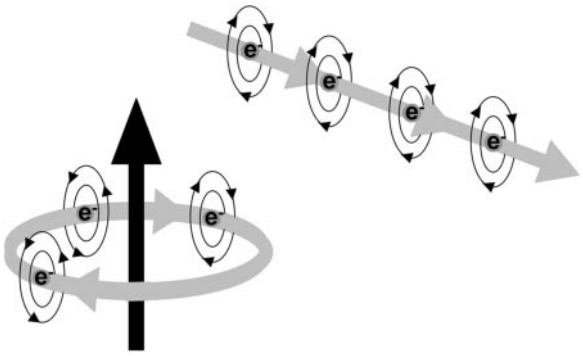


Figure 1. Electrons flowing along a wire. An electric current in a loop of wire will produce a magnetic field (black arrow) perpendicular to the loop of wire. e^- = electron.

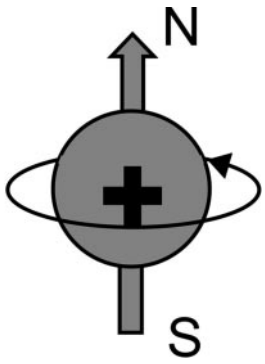


Figure 2. Hydrogen proton. The positively charged hydrogen proton *(+)* spins about its axis and acts like a tiny magnet. *N* = north, *S* = south.

Introduction

For radiologists who interpret magnetic resonance (MR) images, it is extremely important to understand the mechanisms that are used to create the image data. This is especially important in MR imaging, where image contrast can change in a subtle or drastic way depending on how the data are acquired.

This article will provide an introduction to the physics of MR imaging. Some very basic initial concepts will be described, and these will be combined to form the foundation for the more complicated concepts of T1 and T2 relaxation and contrast. Finally, several basic pulse sequences will be discussed.

An attempt has been made to keep the descriptions quite simple; they assume no prior understanding of MR physics, and no complicated math is included. A difficulty remains in the fact that all of the simple concepts must be retained simultaneously in order to apply these concepts to more complicated learning situations.

Initial Concepts

Production of a Magnetic Field

When an electron travels along a wire, a magnetic field is produced around the electron (Fig 1). When an electric current flows in a wire that is formed into a loop, a large magnetic field will be formed perpendicular to the loop.

Resonance

Resonance aids an efficient transfer of energy. This is true, for example, when pushing a child on a swing. The child will swing back and forth at a particular frequency. If we push the swing at the right time, we will efficiently transfer energy to the swing and child. If we consistently push at the right time, we will be in resonance with the swing, and the efficient transfer of energy will allow the child to swing higher.

Hydrogen Protons

It is necessary to have a source of hydrogen protons (protons in the nuclei of hydrogen atoms, which are associated with fat and water molecules) in order to form our MR signal. The hydrogen proton is positively charged and spins about its axis (like a child's spinning top). This positively charged spinning proton acts like a tiny magnet (Fig 2). The hydrogen protons in our body thus act like many tiny magnets.

Main Magnetic Field

The main magnetic field of an MR system comes from a large electric current flowing through wires that are formed into a loop in the magnet of the

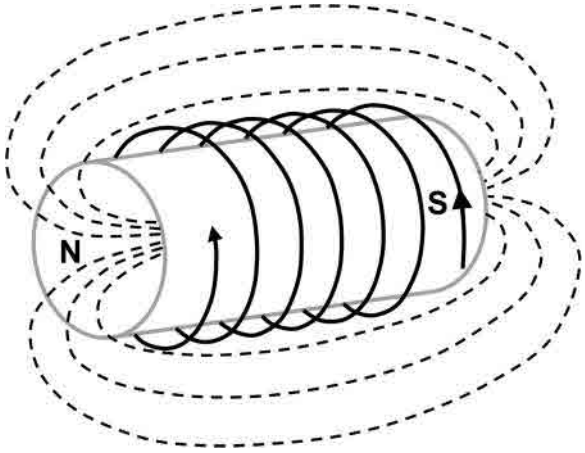


Figure 3. Main magnetic field. A large electric current in loops of wire at superconducting temperatures will produce a very large magnetic field. *N* = north, *S* = south.

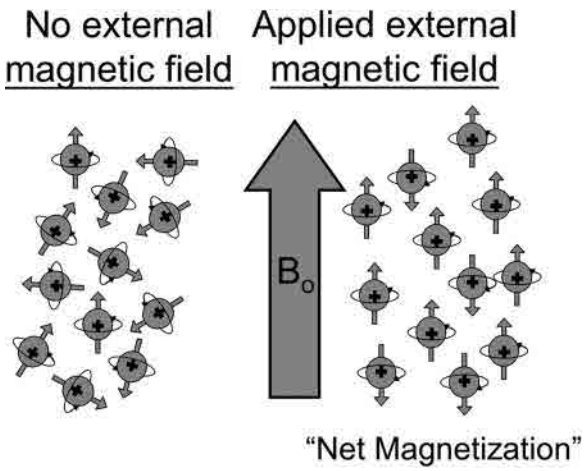


Figure 4. Alignment of protons with the B_0 field. With no external magnetic field, hydrogen protons *(+)* are oriented randomly. When the protons are placed in a strong magnetic field *(B_0)*, a net magnetization will be produced parallel to the main magnetic field.

imaging system (Fig 3). A typical clinical MR system will have a magnetic field strength of 1.5 T (tesla) (1 T = 10,000 gauss). The wires are immersed in liquid helium (at superconducting temperatures) so that very large currents can be used to produce the strong magnetic field. The magnet can be "ramped" with a power supply (to inject electric current into the coils of wire), and the power supply can then be removed. The imaging system can retain this electric current for many years (with no need to inject additional electric

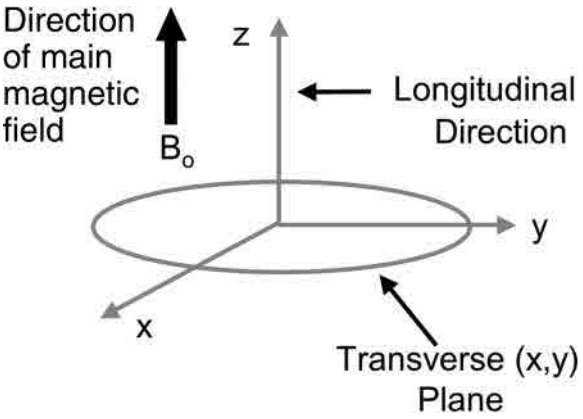


Figure 5. Coordinate system. For a typical 1.5-T cylindrical-bore imaging unit, the z axis (longitudinal direction) is often aligned with the main magnetic field; the plane perpendicular to this is called the transverse plane.

current) with only minimal loss in electric current and minimal decrease in magnetic field strength. The liquid helium levels in the magnet will need to be filled at regular intervals (once per month to once every few years, depending on the magnet design).

Putting these basic elements together, there are protons in the body, positively charged and spinning about their axes, that act like tiny magnets. They are randomly oriented so that their magnetic fields do not sum but rather cancel out (Fig 4). When we place these protons in a strong magnetic field (called B_0), some will tend to align in the direction of the magnetic field and some will tend to align in a direction opposite to the magnetic field. The magnetic fields from many protons will cancel out, but a slight excess of the protons will be aligned with the main magnetic field, producing a "net magnetization" that is aligned parallel to the main magnetic field. This net magnetization becomes the source of our MR signal and is used to produce MR images.

Coordinate System

Because we have just introduced a reference to a direction, it is important to discuss the coordinate system, which will orient us for future discussion. The direction parallel to the main magnetic field is the longitudinal direction, which may also be called the z direction (Fig 5). For typical 1.5-T

superconducting cylindrical-bore magnets, the z direction is horizontal and corresponds to the head-to-foot (or foot-to-head) direction. The plane perpendicular to this direction is called the transverse plane or the x-y plane. For a patient who is headfirst and supine in a superconducting magnet, the x direction is often chosen to be the left-right direction of the patient and the y direction is often chosen to be the anterior-posterior direction. Interestingly, the transverse plane matches the axial plane for typical 1.5-T magnets.

Precession

A spinning top spins about its axis. The force of gravity attempts to pull the top so that it will fall down. The combined effects of gravity and the spinning motion cause the top to precess. The same thing happens with nuclear precession. There are protons that are spinning and acting like tiny magnets. If we place these spinning protons in a strong magnetic field, the force from the magnetic field interacts with the spinning protons and results in precession of the protons (Fig 6).

It is the frequency of precession that is important. How many revolutions in a second does the proton precess? We must know this precessional frequency just as we must know the frequency of the pendulum motion of a child's swing. It is this proton precessional frequency that allows us to create a situation through which the resonance phenomenon can be used to efficiently transfer energy to the protons.

The proton precessional frequency is determined from the Larmor equation, in which the frequency of precession, *f*, is equal to a constant times the main magnetic field strength (Fig 7). The constant is called the gyromagnetic ratio and is a characteristic of each type of nuclei. For hydrogen protons, the gyromagnetic ratio is equal to 42.6 MHz/T (megahertz per tesla). The main magnetic field strength, B_0, depends on the magnet design. For a typical superconducting MR system, the magnetic field strength may be 1.5 T. The frequency of precession then will equal 42.6 MHz/T $\times$ 1.5 T or about 64 MHz (64 million times per second).

Radiofrequency Energy

Radiofrequency (RF) energy comes in the form of rapidly changing magnetic and electric fields generated by electrons traveling through loops of wire with the direction of current flow rapidly changing back and forth at "radio frequencies." The magnetic field (generated by the flow of electrons) will also rapidly change directions. Radio and television stations broadcast at frequencies in units of megahertz, so a broadcast at 89.9 on your FM dial is really at 89.9 MHz. This RF energy is not far from the precessional frequencies of a 1.5-T magnet (64 MHz) and is a reason why MR systems must be shielded from external RF signals.

For the MR system, this RF energy is transmitted by an RF transmit coil (eg, body coil, head coil, knee coil). Typically, the RF is transmitted for a short period of time; this is called an RF pulse. This transmitted RF pulse must be at the precessional frequency of the protons (calculated via the Larmor equation) in order for resonance to occur and for efficient transfer of energy from the RF coil to the protons.

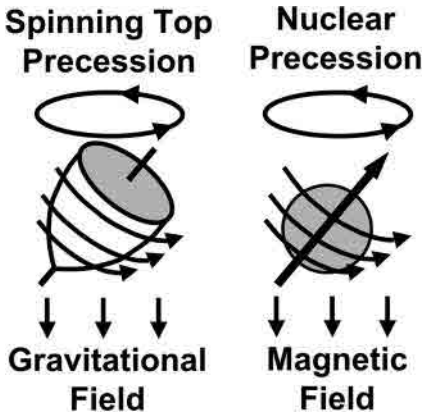


Figure 6. Precession. Precession of a spinning top and nuclear precession are similar in that an external force combined with the spinning motion causes precession.

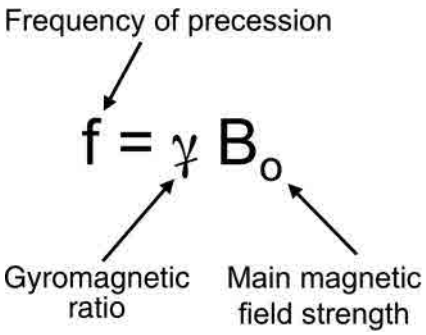


Figure 7. Larmor equation. The Larmor equation allows us to determine the frequency of precession of a proton in a magnetic field.

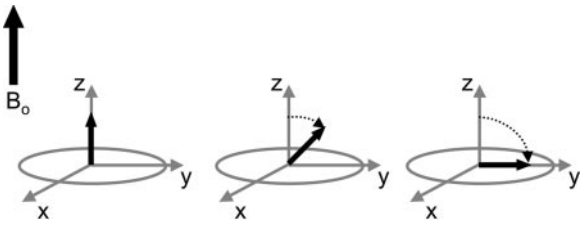


Figure 8. Absorption of RF energy. Left: Prior to an RF pulse, the net magnetization (small black arrow) is aligned parallel to the main magnetic field and the z axis. Center and right: An RF pulse at the Larmor frequency will allow energy to be absorbed by the protons, thus causing the net magnetization to rotate away from the z axis.

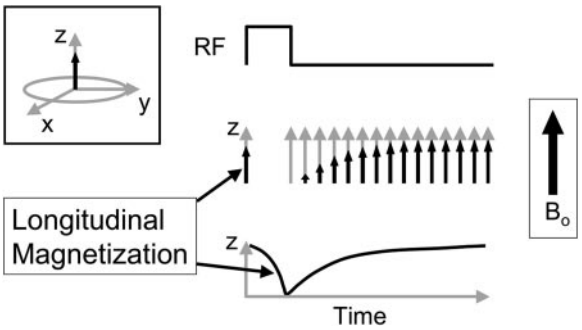


Figure 9. Longitudinal (T1) relaxation. Application of a 90° RF pulse causes longitudinal magnetization to become zero. Over time, the longitudinal magnetization will grow back in a direction parallel to the main magnetic field.

Absorption of RF Energy

Recall that when protons in our body are placed in the vicinity of a strong magnetic field, the magnetic fields from these protons combine to form a net magnetization. This net magnetization points in a direction parallel to the main magnetic field (also called the longitudinal direction). As energy is absorbed from the RF pulse, the net magnetization rotates away from the longitudinal direction (Fig 8). The amount of rotation (termed the flip angle) depends on the strength and duration of the RF pulse.

If the RF pulse rotates the net magnetization into the transverse plane, that is termed a 90° RF pulse. If the RF pulse rotates the net magnetization 180° into the −z direction, that is termed a 180° RF pulse. The strength and/or duration of the RF pulse can be controlled to rotate the net magnetization to any angle. We will see that 90° and 180° RF pulses are important when discussing the spin echo (SE) and that smaller flip angles are important when discussing fast imaging techniques as in gradient-recalled-echo (GRE) imaging.

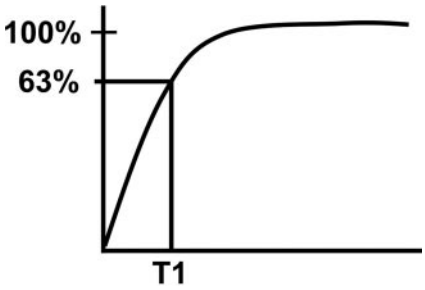


Figure 10. Definition of T1. T1 is a characteristic of tissue and is defined as the time that it takes the longitudinal magnetization to grow back to 63% of its final value.

T1 Relaxation and Contrast

We may now apply the fundamental concepts presented earlier to more complicated MR situations. Net magnetization that is aligned with the longitudinal direction may be called longitudinal magnetization. After a 90° RF pulse rotates the longitudinal magnetization into the transverse plane, this magnetization may be called transverse magnetization. After a 90° RF pulse, the longitudinal magnetization is zero. The magnetization then begins to grow back in the longitudinal direction (Fig 9). This is called longitudinal relaxation or T1 relaxation. The rate at which this longitudinal magnetization grows back is different for protons associated with different tissues and is the fundamental source of contrast in T1-weighted images. T1 is a parameter that is characteristic of specific tissue (and also depends on the main magnetic field strength) and is related to the rate of regrowth of longitudinal magnetization.

The net magnetization does not rotate back up but rather increases in a direction always parallel to the longitudinal direction, which is the direction of the main magnetic field. We can plot an example of this effect (Fig 9). The definition of T1 is the time that it takes for the longitudinal magnetization to reach 63% of its final value, assuming a 90° RF pulse (Fig 10). The magnetization of tissues with different values of T1 will grow back in the longitudinal direction at different rates.

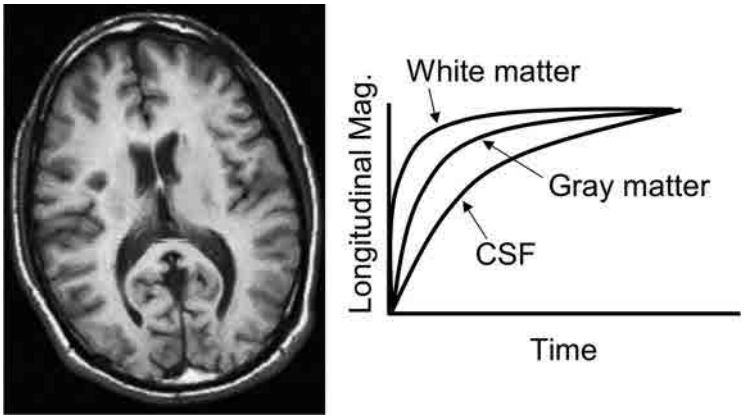


Figure 11. T1-weighted contrast. Different tissues have different rates of T1 relaxation. If an image is obtained at a time when the relaxation curves are widely separated, T1-weighted contrast will be maximized. *Mag* = magnetization.

White matter has a very short T1 time and relaxes rapidly. Cerebrospinal fluid (CSF) has a long T1 and relaxes slowly. Gray matter has an intermediate T1 and relaxes at an intermediate rate (Fig 11). If we were to create an image at a time when these curves were widely separated, we would produce an image that has high contrast between these tissues. Thus, white matter contributes to the lighter pixels, CSF contributes to the darker pixels, and gray matter contributes to pixels with intermediate shades of gray. This type of contrast mechanism is termed T1-weighted contrast. If we were to create an image at a time when the curves were not widely separated, the image would not have much T1-weighted contrast.

T2 Relaxation and Contrast

The description of T2 (or transverse) relaxation begins with the net magnetization aligned with the z direction and a 90° RF pulse that rotates this net magnetization into the transverse plane (Fig 12). Recall that the net magnetization is made up of contributions from many protons, which are all precessing. During the RF pulse, the protons begin to precess together (they become "in phase"). Immediately after the 90° RF pulse, the protons are still in phase but begin to dephase due to several effects. These effects are listed in the Table.

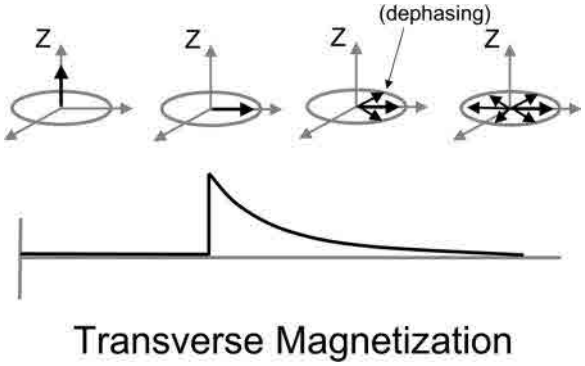


Figure 12. Transverse (T2*) relaxation. Immediately after application of a 90° RF pulse, transverse magnetization is maximized; it then begins to dephase due to several processes (Table). The signals from these dephasing protons begin to cancel out, and the MR signal decreases.

Effects That Cause T2* and T2 Dephasing

Causes of T2* Dephasing	Causes of T2 Dephasing
Spin-spin interactions	Spin-spin interactions
Magnetic field inhomogeneities	
Magnetic susceptibility	
Chemical shift effects	

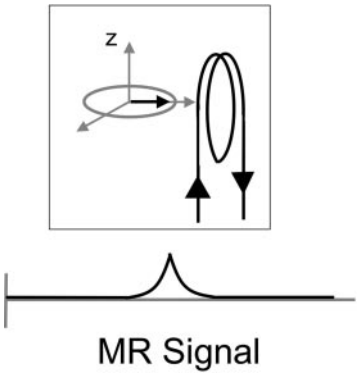


Figure 13. Measurement of the MR signal. A magnetic field (black arrow) that is near and perpendicular to a loop of wire will produce an electric current in the loop. The current can be digitized and stored for later reconstruction into an MR image.

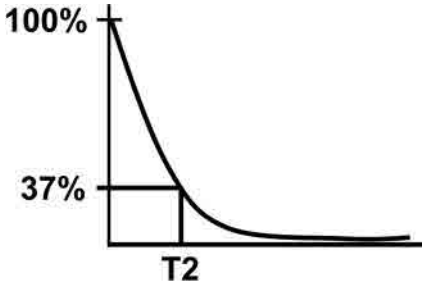


Figure 14. Definition of T2. T2 is a characteristic of tissue and is defined as the time that it takes the transverse magnetization to decrease to 37% of its starting value.

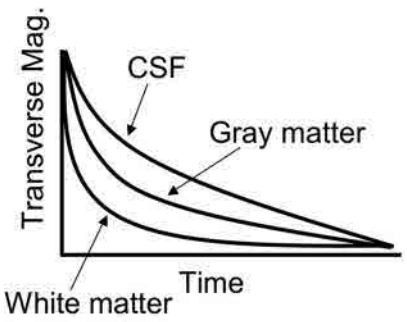
Dephasing due to one of these effects (magnetic field inhomogeneities) will be discussed. Recall that the Larmor equation allows us to determine the precessional frequency of a proton as the product of the gyromagnetic ratio and main magnetic field strength. The gyromagnetic ratio is a constant; however, owing to hardware limitations, the main magnetic field is not perfectly homogeneous across the imaging volume. Thus, protons that experience slightly different magnetic field strengths will precess at slightly different Larmor frequencies. Protons that were in phase immediately after the 90° RF pulse, because they are precessing at slightly different frequencies, will begin to dephase.

Dephasing normally occurs due to all four effects, and in this case, the dephasing may be called T2* (T2 star) decay or T2* relaxation. The dephasing due to three of the effects can be reversed through a special "trick" discussed later. In this case, when dephasing is due only to the effect called spin-spin interactions, the dephasing may be called T2 decay or T2 relaxation. T2 is a parameter that is characteristic of specific tissue and characterizes the rate of dephasing for the protons associated with that tissue.

We can measure the amount of transverse magnetization with a receiver coil. Recall that an electric current in a wire will produce a magnetic field perpendicular to the loop of wire. Measurement of the transverse magnetization (which is our "MR signal") occurs through an opposite effect. In this case, the transverse magnetization, which is a magnetic field, can induce a current in a loop of wire (Fig 13). This induced electric current is then digitized and recorded in the computer of the MR system for later reconstruction as an MR image.

When the transverse magnetization is completely in phase, our measured MR signal is at a maximum. When the transverse magnetization begins to dephase, our measured MR signal begins to decrease until the magnetization is completely dephased, at which time the measured MR signal is zero (Fig 12).

The definition of T2 is the time that it takes for the transverse magnetization to decay to 37% of its original value (Fig 14). Different tissues have different values of T2 and dephase at different rates. White matter has a short T2 and dephases rapidly. CSF has a long T2 and dephases slowly.



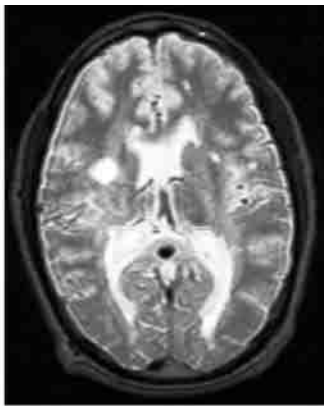
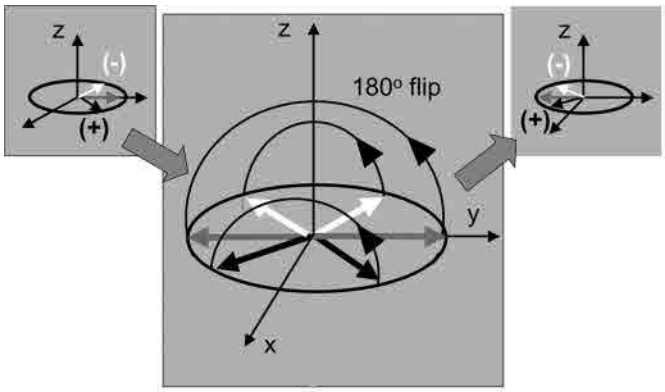
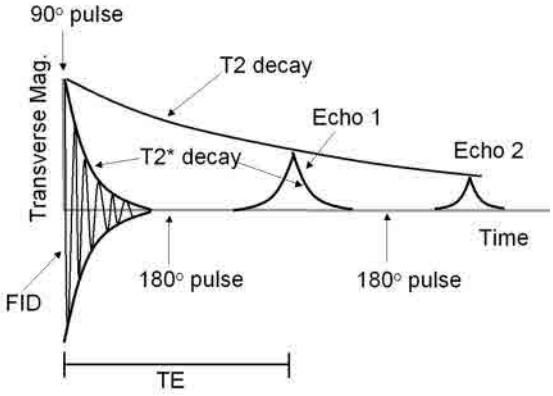


Figure 15. T2-weighted contrast. Different tissues have different rates of T2 relaxation. If an image is obtained at a time when the relaxation curves are widely separated, T2-weighted contrast will be maximized. *Mag* = magnetization.



16.



17.

Figures 16, 17. **(16)** Mechanism of spin echo. After transverse magnetization has begun to dephase in the transverse plane, application of a 180° RF pulse will rotate the proton spins to the opposite axis. This rotation will allow the spins to rephase and form an echo. **(17)** Formation of spin echoes. Application of a 90° RF pulse results in an immediate signal (called a free induction decay [*FID*]), which rapidly dephases due to T2* effects. Application of a 180° RF pulse will allow formation of an echo at a time *TE*. Multiple 180° pulses will form multiple echoes. *Mag* = magnetization.

Gray matter has an intermediate T2 and dephases intermediately (Fig 15).

We are able to take advantage of these differences and produce images based on this contrast mechanism, called T2-weighted contrast. If we were to create an image at a time when the transverse magnetization curves were widely separated, then we would have high contrast between the tissues in our image. We would see that CSF is associated with lighter pixels, white matter is associated with darker pixels, and gray matter is associated with intermediate gray-level pixels. If we were to create an image at a time when the curves were not widely separated, the image would not have much T2-weighted contrast.

The T1 and T2 relaxation processes occur simultaneously. After a 90° RF pulse, dephasing of the transverse magnetization (T2 decay) occurs while the longitudinal magnetization grows back parallel to the main magnetic field. After a few seconds, most of the transverse magnetization is dephased and most of the longitudinal magnetization has grown back.

Spin Echo

The spin echo is the "trick" that can be used to recover dephasing due to all effects except spin-spin interactions. After a 90° RF pulse, protons that were in phase begin to dephase in the transverse plane due to effects discussed earlier (represented by some spins going faster than the average and some spins going slower than the average) (Fig 16). After a certain amount of time, if a 180° RF pulse is applied, the spins will rotate over to the opposite axis. Now, rather than the spins continuing to dephase, the spins will begin to rephase.

The spins will come back together and the signal measured with our receiver coil will increase, form a maximum signal, and then decrease as the spins once again dephase (Fig 17). At this time,

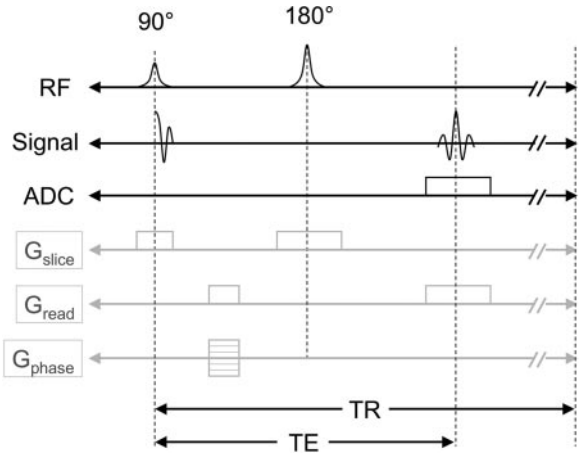


Figure 18. Pulse sequence diagram. A pulse sequence diagram can be used to show the relative timing of certain events during an MR imaging acquisition. The timing of RF pulses, the signal formed from these pulses, and the digitization of the signal is shown. TE is shown as the time to the echo, and the repetition time *(TR)* is shown as the time it takes to go through the pulse sequence once. This pulse sequence uses a 90° RF pulse with a 180° RF pulse to rephase spins to form an echo. T1- and T2-weighted images may be created with this pulse sequence. *ADC* = analog-to-digital converter; in all pulse sequence diagrams, *G* = gradient.

another 180° RF pulse could be applied to rephase the spins again. The rephasing of the spins forms an "echo" called a spin echo. The time between the peak of the 90° RF pulse and the peak of the echo is called the time to echo or echo time (TE). Note that the curve formed by connecting the peaks of the echoes represents decay by T2 effects (spin-spin interactions), whereas the initial faster decay observed immediately after the 90° RF pulse or during echo formation is due to T2* effects (which include all decay processes listed in the Table).

What has not been explained is why decay due to three of the processes can be reversed, but decay due to one process, spin-spin interactions, cannot be reversed. We will continue with the example of magnetic field inhomogeneities to explain this. Although the magnetic field is not perfectly homogeneous, the imperfections remain constant over time and do not move in their position. We take advantage of this with the spin echo and 180° RF pulse.

If a proton experiences a local increase in magnetic field strength that is not experienced by a neighboring proton, it will precess faster than its neighbor. Because this imperfection in the magnetic field is constant, the proton will always spin faster than its neighbor. Prior to the 180° RF pulse, the proton spins faster "away" from its neighbor. After the 180° RF pulse, the spins are "flipped" and their directions can be thought to be reversed, so that now the faster proton is "behind" its neighbor and can "catch up" to its neighbor because it is still spinning faster. On the other hand, spin-spin interactions are random interactions between protons that cause random local changes in the magnetic fields experienced by the protons, and this causes dephasing. Because this is a random process, dephasing due to this effect cannot be reversed.

Referring to Figures 14 and 15 for T2 decay, similar figures could be drawn showing T2* decay. As discussed later, an echo can be produced without application of a 180° RF pulse by using gradients alone. In this case, the rate of rephasing and dephasing of the echo would be due to all effects listed in the Table. If we were to create an image at a time when the transverse magnetization curves were widely separated, then we would have high T2*-weighted contrast between the tissues in our image.

Pulse Sequence Diagrams

We have discussed fundamental concepts and have used those to describe T1 and T2 relaxation and contrast. For MR imaging, we need to learn how to create and control this contrast. This can be done by describing the MR pulse sequence, which shows the timing of certain events during MR acquisition.

The events that will be discussed include RF pulses and the signal that is formed from these pulses. Other events that are included in pulse sequence diagrams are the timing of gradient pulses. Gradient pulses will be described in detail in a future article in this series. They are responsible for localizing the "signals" from protons (which are located in the body at different positions) in our images in three dimensions, through the formation of image sections and pixels in those sections. The timing of the gradient pulses will be included in the figures of pulse sequences (in gray).

The horizontal lines in the pulse sequence diagram of Figure 18 indicate the relative timing of events. Lines are shown for the timing of RF pulses, the signal formed from these pulses, and when the signal is digitized for storage in the acquisition computer by the analog-to-digital converter (ADC).

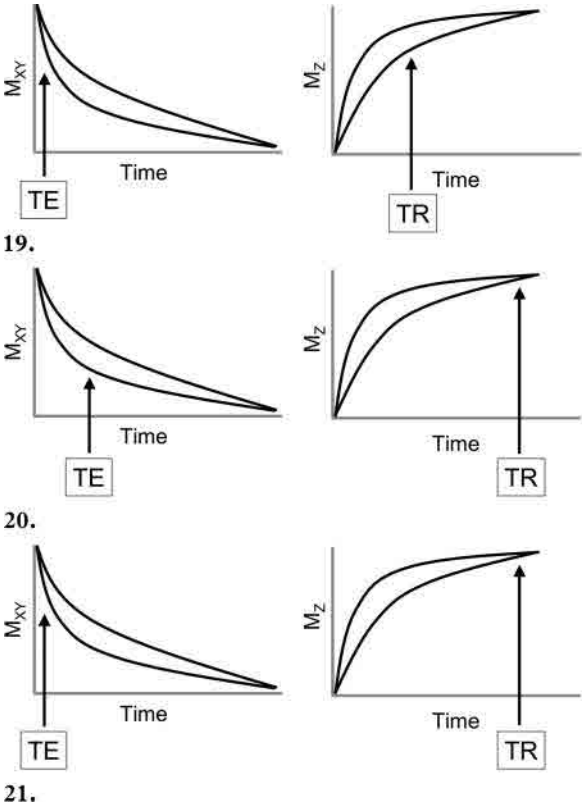
TE and TR

Initially, it is of primary importance to use the pulse sequence diagram (Fig 18) to describe the MR image acquisition parameters TE and TR. TE has already been described as the time between the peak of the 90° RF pulse and the peak of the echo that is formed. Note that the 180° RF pulse occurs at half of the echo time TE. A parameter not yet discussed is the repetition time or TR. TR is the time that it takes to run through the pulse sequence one time.

A subsequent article will discuss how the raw image data are collected and reconstructed to form an image. For now, we will assume that the raw data have the same number of rows and columns as the reconstructed image. For basic pulse sequences, one time through the pulse sequence provides one row of raw data. We must repeat the pulse sequence as many times as necessary to provide as many rows of data as are needed to reconstruct the image. If we wish to acquire an MR image with a matrix of 256 pixels by 256 pixels, that is 256 rows of data and 256 columns of data. Because one time through the pulse sequence provides one row of data (in 256 columns), we must repeat the pulse sequence 256 times to acquire all the rows needed. TR is the time it takes to go through the pulse sequence one time. In order to acquire all rows of data, it will take a time equal to TR times 256.

Contrast Formation

Recall that the goal of MR imaging is to create images that have certain contrasts. From Figures 11 and 15, we see how the longitudinal and transverse magnetizations relax due to T1 and T2 effects. TE and TR can be used to control the amount of "weighting" of these effects in our image. Figures 19–21 show the relative values of TE and TR to produce these different image contrast weightings. When effects from T2 relaxation are minimized (curves not widely separated) and effects from T1 relaxation are maximized (curves widely separated), we would produce a T1-weighted image (Fig 19). If T1 effects are minimized and T2 effects are maximized, we would produce a T2-weighted image (Fig 20). If both T1 and T2 effects are minimized, we will produce an image with "proton density" or "spin density" weighting (Fig 21).



Figures 19–21. **(19)** Parameters for T1 weighting. Short TE (producing minimal T2 weighting) and intermediate TR (producing maximal T1 weighting) will result in a T1-weighted image. **(20)** Parameters for T2 weighting. Long TE (producing maximal T2 weighting) and long TR (producing minimal T1 weighting) will result in a T2-weighted image. **(21)** Parameters for proton density weighting. Short TE (producing minimal T2 weighting) and long TR (producing minimal T1 weighting) will result in a proton density–weighted image.

Basic Pulse Sequences

Several basic pulse sequences will now be discussed. The first pulse sequence will be the spin-echo sequence. Other pulse sequences will be compared to the spin-echo sequence; the figures will highlight the differences between that pulse sequence and the spin-echo sequence.

Spin Echo

The spin-echo pulse sequence (Fig 18) can produce proton density weighting, T1 weighting, and T2 weighting. TE and TR are set as discussed earlier to achieve these weightings. Typical values of TE and TR for T1 weighting (at 1.5 T) are TE = 20 msec and TR = 500 msec; the typical

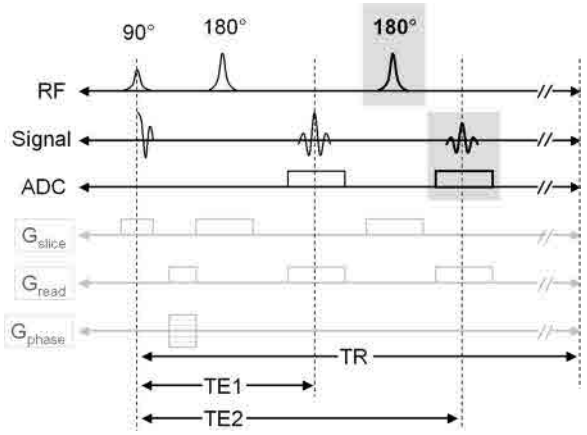


Figure 22. Multiecho spin-echo pulse sequence. This sequence uses a 90° RF pulse with multiple 180° RF pulses to form multiple echoes. Each echo can be used to create a separate image data set with different contrast weighting. The gray highlighting shows the differences between this pulse sequence and the basic spin-echo sequence.

values for T2 weighting are TE = 80 msec and TR = 2,000 msec. Comparing this figure to Figure 17, we see that the 90° RF pulse produces an initial signal (free induction decay), which is not used. The 180° RF pulse occurs at half the TE time, and the echo is centered at TE. The ADC (analog-to-digital converter) line indicates that the echo is digitized and stored in the computer as raw data.

Multiecho Spin Echo

The multiecho spin-echo pulse sequence uses multiple 180° RF pulses to generate multiple echoes (Fig 22). Each echo occurs at a different TE and is used to form a separate image data set, which will have different contrast weighting ranging from proton density to T2. The differences between this pulse sequence and the basic spin-echo pulse sequence are highlighted in Figure 22. Typical TR may be 2,000 msec, with TE1 = 20 msec and TE2 = 80 msec, resulting in proton density– and T2-weighted image data sets, respectively.

Turbo Spin Echo

The turbo spin-echo (or fast spin-echo) pulse sequence is shown in Figure 23. Note the differences here compared to the basic spin-echo pulse sequence. Again, multiple 180° pulses are used to create multiple echoes. However, instead of each

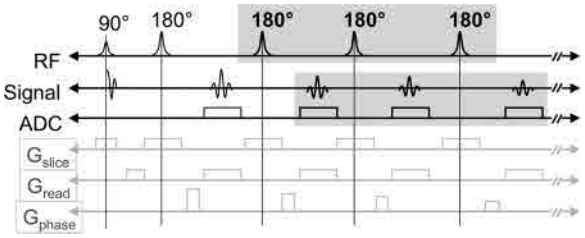


Figure 23. Turbo spin-echo pulse sequence. This sequence uses a 90° RF pulse with multiple 180° RF pulses. Multiple echoes are formed, and the data are used to create a single data set. Multiple rows of raw data are filled during one TR period; this feature allows the pulse sequence to be run fewer times, thus saving imaging time.

echo forming a different image data set, all the echoes are used to create a single image data set at a faster rate. A new acquisition parameter will be introduced called the echo train length, which is the number of echoes that are formed.

Recall that the echo is digitized and the data from this echo are used for one row of raw data. Recall also that the pulse sequence must be repeated as many times as is needed to acquire all the rows of raw data. In the turbo spin-echo sequence, if four echoes are produced (each time through the pulse sequence), the digitized data from these four echoes can be used for four different rows of raw data. If 256 rows of raw data are needed, and four rows of raw data are acquired each time through the pulse sequence, then the sequence must be repeated only 64 times rather than 256 times. With TR the same as in a spin-echo sequence, this would result in a factor of four speed increase in data acquisition. Likewise, an echo train length of eight or 16 will decrease imaging time by a factor of eight or 16, respectively.

The turbo spin-echo pulse sequence can be used to produce T1 and T2 contrast weighting. Each echo will still occur at a different TE and thus will really have a different contrast weighting associated with it. However, there is a way that we can use the echoes closest to our TE of interest to form the contrast weighting that we desire. This will become more clear when we understand how the raw data are acquired and used to form an image (explained in a later article).

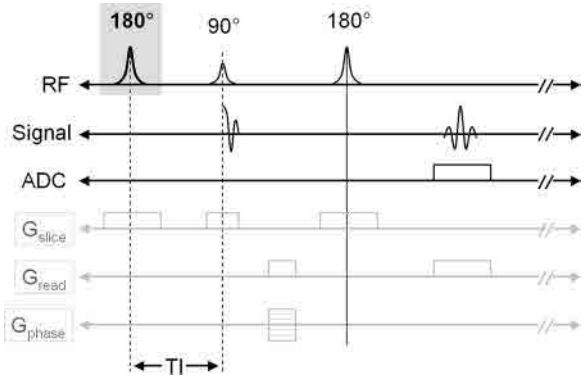


Figure 24. Inversion-recovery pulse sequence. This sequence is similar to the basic spin-echo sequence with the addition of an initial 180° inversion pulse. This sequence can be used to suppress the appearance of unwanted signals (eg, those due to fat or fluid). *TI* = inversion time.

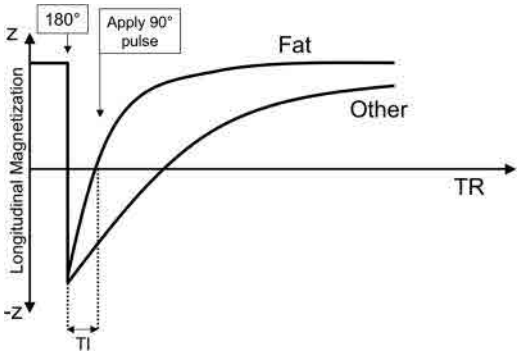


Figure 25. Inversion of the signal in the inversion-recovery sequence. After initial inversion of the longitudinal magnetization, T1 relaxation occurs and the signals from different tissues cross the zero axis at different times. When the signal to be suppressed crosses the zero axis, a 90° RF pulse will rotate all other signals into the transverse plane for image formation. *TI* = inversion time.

Inversion Recovery

The inversion-recovery pulse sequence (Fig 24) is useful for suppressing unwanted signals in MR images (eg, signals from fat or fluid). Contrast weighting can still be controlled through selection of TR and TE, as described earlier.

The difference between this and the spin-echo pulse sequence is the occurrence of the 180° RF pulse prior to the regular spin-echo pulse sequence. The 180° RF pulse causes an initial inversion of the longitudinal magnetization (so that it is aligned in the −z direction), as shown in Figure 25. The magnetization then begins to grow back in the direction of the main magnetic field (+z). The magnetization of different tissues will grow back at different rates. When the signal from the tissue to be suppressed crosses the zero axis, application of a 90° RF pulse will rotate all other signals into the transverse plane. Since the signal from the tissue at the zero point is zero, there is nothing to rotate into the transverse plane. Thus, this tissue will not contribute any brightness to the resulting image.

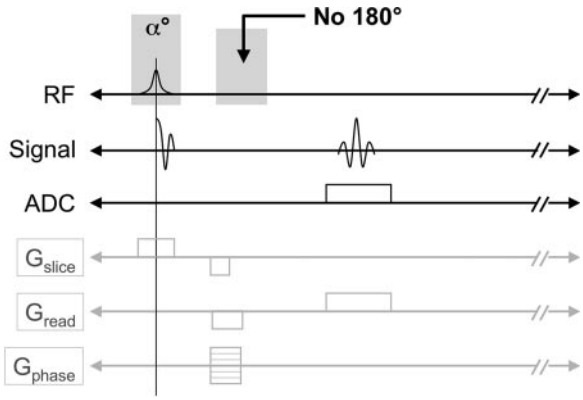


Figure 26. Gradient-recalled-echo pulse sequence. This sequence is similar to the spin-echo sequence except that the initial RF pulse is less than 90° and there is no 180° RF pulse. Signal dephasing and rephasing by means of gradient pulses results in formation of a gradient echo, which is used to produce T1- or T2*-weighted images.

The acquisition parameter TI (time of inversion) is the time between the initial 180° RF pulse and the 90° RF pulse. Fat relaxes relatively quickly, and a short TI of approximately 170

msec is used to suppress signal from fat at a field strength of 1.5 T. This method can also be used to suppress signal from other tissues that cross through the zero point by appropriate application of TI for that tissue.

Gradient Recalled Echo

Finally, the pulse sequence diagram for the gradient-recalled-echo sequence is shown in Figure 26. Initial inspection shows the difference between this sequence and the basic spin-echo sequence to be an initial RF pulse flip angle of something less than 90° (eg, 20° or 30°) and the lack of a 180° RF pulse. The smaller flip angle and lack of 180° RF pulse allow the TR to be much shorter, resulting in very fast imaging times. Even though there is no 180° RF pulse to produce a spin echo, gradient pulses (which we have not discussed) can be used to dephase and rephase the signal in the transverse plane to form gradient echoes. In this case, T2-weighted image contrast cannot be produced; rather, T1 and T2* image contrast can be produced.

Conclusions

Many concepts fundamental to an understanding of MR imaging have been presented. It will be important for those new to this imaging modality to review these concepts and be able to apply these to more complicated situations in MR imaging. Some basic core elements of MR imaging were initially discussed, and these formed a foundation for subsequent discussion of T1 and T2 contrast mechanisms and several different pulse sequence acquisition strategies. Other topics that remain to be presented in future articles in this series include localization of the MR signal by using gradients, instrumentation, image artifacts, and safety.

Suggested Readings

Bushberg JT, Seibert JA, Leidholdt EM Jr, Boone JM. Nuclear magnetic resonance. In: The essential physics of medical imaging. 2nd ed. Philadelphia, Pa: Lippincott Williams & Wilkins, 2002; 373–413.

Elster A, Burdette J. Questions and answers in magnetic resonance imaging. 2nd ed. St Louis, Mo: Mosby, 2001.

Hendee WR, Ritenour ER. Fundamentals of magnetic resonance. In: Medical imaging physics. 4th ed. New York, NY: Wiley-Liss, 2002; 355–365.

Mitchell DG. MRI principles. Philadelphia, Pa: Saunders, 1999.

Pooley RA, Felmlee JP, Morin RL. Basic principles and terminology of magnetic resonance imaging. In: Berquist TH, ed. MRI of the musculoskeletal system. 4th ed. Philadelphia, Pa: Lippincott Williams & Wilkins, 2001; 1–29.

Runge VM, Nitz WR, Schmeets SH, et al. The physics of clinical MR taught through images. New York, NY: Thieme, 2005.

Wolbarst AB. Magnetic resonance imaging I: nuclear magnetic resonance of stable hydrogen nuclei in the water molecules of tissues. In: Wolbarst AB, ed. Physics of radiology. 2nd ed. Madison, Wis: Medical Physics, 2005; 128–138.

AAPM/RSNA Physics Tutorial for Residents

MR Imaging: Brief Overview and Emerging Applications[1]

Michael A. Jacobs, Ph.D., Tamer S. Ibrahim, Ph.D., Ronald Ouwerkerk, Ph.D.

Reprinted with permission from Radiological Society of North America, Radiographics 2007, Volume 27, Pages 1213 - 1229, © RSNA, 2007

TEACHING POINTS
See last page

Magnetic resonance (MR) imaging has become established as a diagnostic and research tool in many areas of medicine because of its ability to provide excellent soft-tissue delineation in different areas of interest. In addition to T1- and T2-weighted imaging, many specialized MR techniques have been designed to extract metabolic or biophysical information. Diffusion-weighted imaging gives insight into the movement of water molecules in tissue, and diffusion-tensor imaging can reveal fiber orientation in the white matter tracts. Metabolic information about the object of interest can be obtained with spectroscopy of protons, in addition to imaging of other nuclei, such as sodium. Dynamic contrast material–enhanced imaging and recently proton spectroscopy play an important role in oncologic imaging. When these techniques are combined, they can assist the physician in making a diagnosis or monitoring a treatment regimen. One of the major advantages of the different types of MR imaging is the ability of the operator to manipulate image contrast with a variety of selectable parameters that affect the kind and quality of the information provided. The elements used to obtain MR images and the factors that affect formation of an MR image include MR instrumentation, localization of the MR signal, gradients, k-space, and pulse sequences.

©RSNA, 2007

Abbreviations: FOV = field of view, RF = radiofrequency, SNR = signal-to-noise ratio, TE = echo time, TR = repetition time

RadioGraphics 2007; 27:1213–1229 • **Published online** 10.1148/rg.274065115 • **Content Codes:** MR PH

[1]From the Russell H. Morgan Department of Radiology and Radiological Science (M.A.J., R.O.) and Sidney Kimmel Comprehensive Cancer Center, Department of Oncology (M.A.J.), Johns Hopkins University School of Medicine, Traylor Bldg, Room 217, 712 Rutland Ave, Baltimore, MD 21205; the Departments of Radiology and Bioengineering, University of Pittsburgh, Pittsburgh, Pa (M.A.J., T.S.I.); and the School of Electrical and Computer Engineering and Bioengineering Center, University of Oklahoma, Norman, Okla (T.S.I.). From the AAPM/RSNA Physics Tutorial at the 2004 RSNA Annual Meeting. Received June 7, 2006; revision requested August 16; final revision received March 9, 2007; accepted March 9. Supported in part by grants 1R01CA100184 (M.A.J.), P50 CA103175 (M.A.J.), and 1R21CA095907-01 (R.O.) from the National Institutes of Health. All authors have no financial relationships to disclose. **Address correspondence to** M.A.J. (e-mail: *mikej@mri.jhu.edu*).

©RSNA, 2007

Introduction

Magnetic resonance (MR) imaging has been well established as both a diagnostic and research tool in many areas of medicine because of its ability to provide excellent soft-tissue delineation of different areas of interest. For example, in the brain, T1- and T2-weighted MR imaging has evolved to be the standard of reference for anatomic definition. These sequences derive image contrast from the spin density in water and fat and from the MR relaxation parameters T1 and T2. Unfortunately, the water and fat spin densities yield only limited information and present difficulty in separating adipose tissue from nonadipose tissue unless fat saturation is employed. These relaxation parameters can be used in a wide variety of T1- and T2-weighted sequences to optimize contrast for specific diagnostic purposes. For example, T2 provides information about edema within the brain.

The link between the differences in T1 and T2 and the physiology of the various tissues, and, more important, the physiology of diseased tissue, is not always clear. Altering the MR image contrast with an intravascular contrast agent typically reveals physiologic changes in tissue that are relevant to disease processes. For example, contrast agents, such as gadolinium, administered to the bloodstream create more contrast in highly vascular regions and are retained in regions where the permeability of the interstitial space has changed. These types of changes in vascularity or tissue permeability occur in a variety of diseased tissues, such as malignant tumors and myocardial ischemia.

MR imaging plays an increasingly important role in radiologic imaging of different pathologic disorders, where the goal is developing radiologic imaging markers for noninvasive prediction of disease and response to treatment. For example, MR imaging used in oncologic imaging consists of anatomic T1- and T2-weighted sequences, dynamic contrast material enhancement (1,2), or MR spectroscopy in the brain (3–7), breast (8–13), and prostate (14,15). Dynamic contrast enhancement with gadolinium yields information on the vascular status of a lesion, and MR spectroscopy probes the intracellular (eg, choline, creatine) environment of tissue (16). When these sequences are combined, they can assist the physician in making a diagnosis or monitoring a treatment regimen.

One of the major advantages of the different types of MR imaging is the ability of the operator to manipulate image contrast with a variety of selectable parameters that affect the kind and quality of the information provided. Therefore, this article reviews the elements that are used to obtain MR images and the factors that affect the formation of an MR image—specifically, instrumentation, localization of the MR signal, gradients, k-space, and pulse sequences—as well as emerging applications in high-field-strength MR imaging (17–22).

MR Instrumentation

The generation of MR images requires a sophisticated combination of electronics, radiofrequency (RF) generators, coils, and gradients that interface with a computer for communication between the different electronics. This combination of equipment allows localization, excitation, and acquisition of a specific tissue of interest and formation of a digital image. There are two groups of equipment that are combined to form the MR system. The first group is a command and control center, that is, the computer, interface, and data storage. The second group is specialized equipment that generates and receives the MR signal, that is, the magnet, gradients, and RF coils. This article gives only a brief introduction; the reader is referred to several references (23–29) and excellent textbooks (30–38) for a more detailed explanation of these topics.

Magnets

The magnet provides the "external" magnetic field in which the patient or object is placed, and its performance requirements are usually defined in terms of field strength, stability, and homogeneity (34,39). There are three types of magnets that can be used in MR imaging: permanent, resistive, and superconducting.

Permanent Magnets.—Permanent magnets exploit the ferromagnetic properties of the metal used (eg, iron, nickel, or other metals). They are configured differently from resistive and superconducting magnets. Specifically, the main magnetic field (B_0) of a permanent magnet is perpendicular to the object of interest, and early permanent magnets were very heavy (5–100 tons). However, newer versions are lighter and are sometimes used for limited clinical applications

such as open magnets. Advantages of permanent magnets are that they require no cooling or power to run and thus are cheaper than the other magnets. However, they cannot be turned off in emergencies and have less field homogeneity (34,38).

Resistive Magnets.—Recall that when an electric current flows through a wire, a magnetic field is induced around the wire based on the Maxwell equations; this principle is used for construction of a resistive magnet. Resistive magnets require cooling and power to operate but can be turned off and on (31–34). Their field strengths range from 0.1 T to 0.3 T, and they have the disadvantages of poor homogeneity and high electrical costs (34–36,38). Also, the object of interest lies parallel to the B_0 field, and the usual application is similar to that of permanent magnets in the "open magnet" configuration.

Superconducting Magnets.—Superconducting magnets are based on the principle of cooling down (~4°K) certain metal conductors so that there is little or no resistance; therefore, a high electric current can be used to generate high-strength magnetic fields (Maxwell equation) with no major heat disposition. However, in order to achieve small electrical resistance, expensive cooling cryogens (usually liquid helium) are used (31–34). Currently, most clinical systems use superconducting magnets with field strengths of 0.5–3 T, with most field strengths on the order of 1.5–3 T. Research magnets (clinical or experimental) can have field strengths of 4–9.4 T (17–21).

Field Strength

The field strength of an MR system is a major determinant of the image contrast due to the energy exchange between the protons (water) and their environments. These interactions are governed by the magnetic moments of the protons, in particular the longitudinal relaxation parameter T1 (discussed later) (29,30). The time required for complete relaxation differs for different field strengths; for example, the T1 is shorter at lower field strengths and tends to increase at higher field strengths (29,30). These changes affect both the signal- and contrast-to-noise ratios of MR images (discussed later) (39–41).

The units of field strength of an MR system are tesla or gauss, with 1 T equal to 10,000 G. As discussed earlier, the range of magnetic field strength is variable, from low (0.1–0.5 T), medium (0.5–1.0 T), or high (1.5 T) to ultrahigh (3.0 T or greater) (29,33,42). Although there have been vast technological advances in MR imaging over the past 40 years, the central principle for advancing the MR imaging technology has been based on finding ways to increase signal-to-noise ratio (SNR) (40,41) in the MR image or spectra. The most fundamental approach to boosting SNR has been to increase the field strength of the MR magnets. As a result, human MR imaging is currently performed at field strengths reaching 4 T (17), 7 T (21,43), 8 T (44,45), and 9.4 T (46).

Shim and Gradient Coils

The localization of the MR signal depends on good local homogeneity (shim) of the magnetic field and variation (gradient) of the magnetic field in three different directions. This is accomplished by using both shim and gradient coils with the magnet. Basically, a shim or gradient coil is a device that can generate a spatially localized magnetic field within the main B_0 field by using electric current. Physically, the shim and gradient coils are placed concentric to each other in the magnet and activated at specific times of the pulse sequence.

Shim Coils.—The quality of the received signal requires good field homogeneity and thus requires a shim of the local magnetic field, which is the B_0 field along the z direction. When an object is placed in the main B_0 field, it creates local susceptibility effects, and these susceptibility effects need to be corrected. Shim coils (also known as correction coils) are used to adjust or "shim" B_0 magnetic field inhomogeneities and are very important for the quality of the received signal (33,34,36–38). The shim coils can be passive or active, depending on the configuration of the magnet. Passive shim coils are usually configured at the time of installation of the magnet by using metal plates within the bore or surface of the magnet. Active shim coils require electric current through special coils and provide additional "shimming" around the object of interest. Most clinical and research systems use both passive and active shims for control of the local magnetic field.

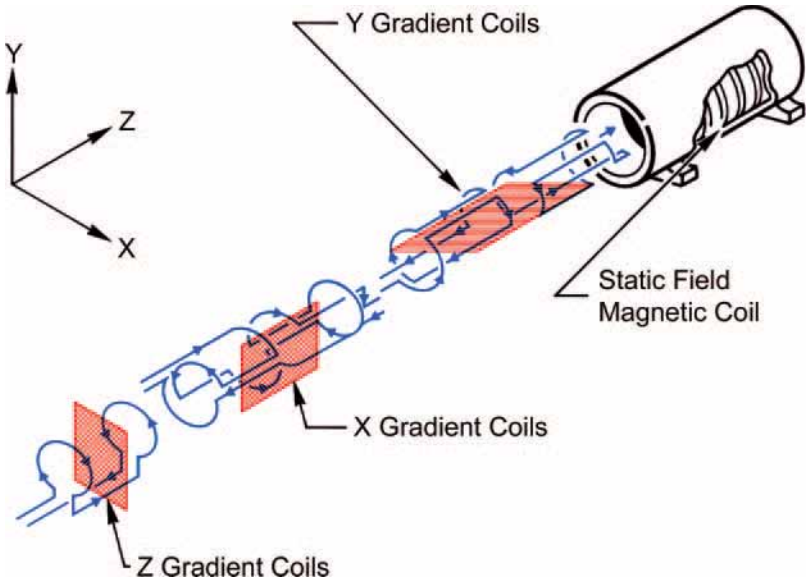


Figure 1. Typical gradient coil set used for localization of the MR signal. These coils are placed concentrically to each other within the magnet and are used sequentially for three-dimensional localization of the gradients to create images from the MR signal.

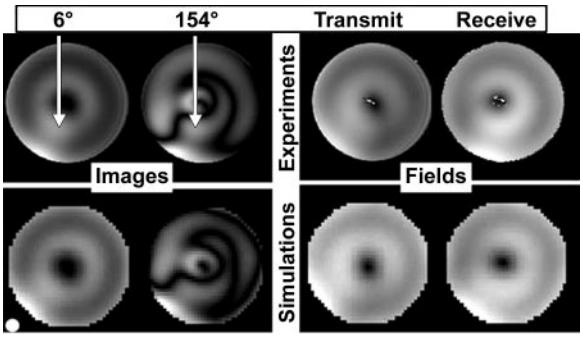
Gradient Coils.—Gradient coils are used for localization of the MR signal in three directions (x, y, and z) by using a controlled linear variation (changing) of the B_0 magnetic field with distance (24,33,34,36–38). This linear variation of the magnetic field allows spatial localization of the MR signal. These coils lie concentric to each other and are used to obtain the MR images. Important parameters for gradient specification are the amplitude, rise time, and slew rate of gradient systems. The amplitude or gradient strength is defined as tesla per meter or gauss per centimeter, with 10 mT/m = 1 G/cm. The rise time (in milliseconds) is how long it takes for the gradient system to reach its maximum strength. The slew rate of a gradient system (in tesla per meters per second) is defined as the ratio of gradient strength divided by the rise time. A typical gradient coil set is shown in Figure 1. The gradients are very important in imaging quality and image formation and are discussed further later in this article.

RF Coils

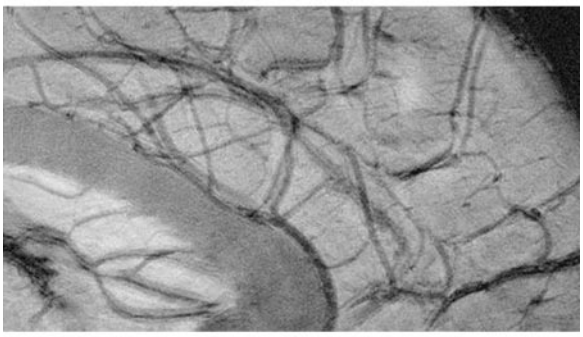
The RF coils are used for two purposes: to transmit the RF energy to the tissue of interest and to receive the induced RF signal from the tissue of interest. They are placed concentric to each other and to the gradient coil system. RF coils are the "antenna" of the MR imaging system. There are several different types of RF coils. Some are transmit or receive only or a combination of both transmit and receive. The type of coil is governed by the desired application, and the RF coil configuration can be varied; usual designs are surface, saddle, quadrature, or phased array (multiple elements). These coils can be designed for the brain, breast, or other body organs.

Therefore, the RF signal is generated by a transmit RF coil and applied to an area of interest, and the output signal is picked up by the RF receive coil and transmitted to an RF amplifier for reconstruction of the image in the main computer (23). However, with the increase in magnetic field strength (~7 T), the principles of building RF coils will change due to the interaction of the magnetic field with the electric field as determined by the Maxwell equations (discussed later).

Multiple RF Coils.—So far, we have discussed the use of only single RF coils. However, use of a greater number of coil elements (or channels) has led to recent technological advances in pulse sequence design and image processing by using parallel imaging methods (simultaneous acquisition of spatial harmonics [47] or sensitivity encoding [48]). These methods have resulted in reduced imaging time but also in a decrease in SNR and are discussed later in this article.



a.



b.

Figure 2. **(a)** Low- and high-flip-angle (arrows) images and measured transmit and receive fields obtained by using an 8-T system (top row) and corresponding simulated results obtained at 340 MHz by using computational electromagnetics (bottom row) (49). **(b)** In vivo 2000 × 2000 image of the human brain obtained at 8 T with 100-μm resolution (20). High-field-strength magnets are increasingly being used in MR imaging research centers throughout the world.

High-Field-Strength RF Coils and Field Distribution.—Higher field strengths correspond to increased operational frequencies, where the wavelengths of the electromagnetic waves produced by currents on RF coils or arrays become on the order of the size of the human head or body, which will result in inhomogeneous B_1 field (further subdivided into B_1+ and B_1-) distributions in biologic tissues. Both of these fields can have a devastating effect on the integrity of the images and on the safety of the patient. Demonstration of these issues is presented in Figure 2, where comparisons between experimental and simulated low- and high-flip-angle images and transmit and receive fields for a coil loaded with a head-sized sphere filled with homogeneous saline are shown at 8 T (45). These results demonstrate the complexities and inhomogeneities of the B_1+ and B_1- field distributions, which can lead to asymmetric and distinctive high-power images even though the coil, load, and excitation possess physical symmetry (45). However, high resolution within the brain can be achieved, as demonstrated in Figure 2b.

Localization of the MR Signal

Background

When a subject or object is placed into a magnetic field, the protons align to the main field (B_0) in the z direction and the Larmor frequency is field dependent (eg, Larmor frequency $\omega = \gamma B_0$, where $\gamma = 42.6$ MHz/T and is called the gyromagnetic ratio). Localization of the MR signal is obtained by applying a gradient that produces a controlled linear spatial variation of the B_0 magnetic field (z direction), which creates small perturbations to the field in three directions (x, y, and z) (Fig 1). This linear magnetic field gradient is defined as any linear, spatial variation of the magnetic field in the z direction in any of the three directions. Usually, the gradients vary in a linear manner over the field of view (FOV) and are defined as the rate of change of the magnetic field (B) in the direction of interest. In all, the gradients perform three functions: slice selection (z component), frequency encoding (x component), and phase encoding (y component).

Teaching Point

Note that each gradient is generated by a separate concentric coil (Fig 1). Typical gradient system values range from 20 to 80 mT/m (1.5 T and 3 T) with increased slew rates from 30 to 220 mT/m/msec, where the slew rate is defined as the maximum gradient divided by the rise time. (The rise time is how long it takes for the gradient to go from zero to the maximum value.)

The linear dependence of the magnetic field B_i depends on the location within the magnet and is defined by the following equation:

$$B_i = B_0 + G \cdot r_i, \qquad (1)$$

where B_i = the magnetic field at r_i and G is the

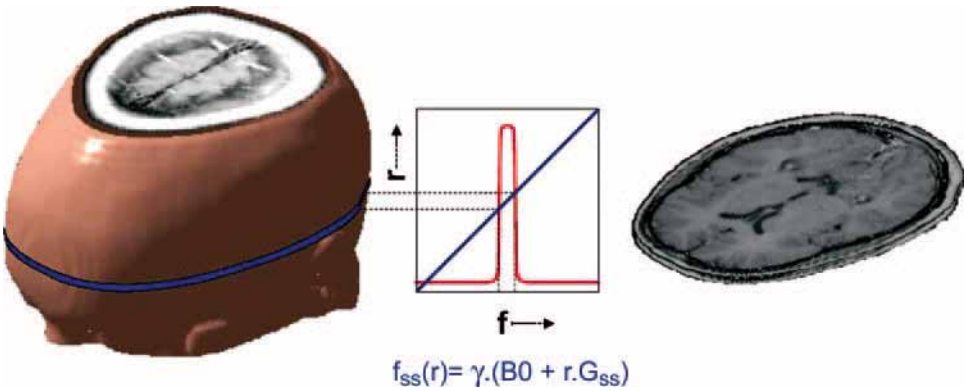


Figure 3. Slice selection by using the slice-selection gradient with a B_0 field gradient and a frequency-selective RF pulse.

total gradient in the chosen direction. For example, the linear dependence in the x direction is as follows:

$$B_x = B_0 + G \cdot r_x. \quad (2)$$

The variation in Larmor frequency, which is the resonant frequency, caused by application of the gradient is defined by the following equation:

$$\omega_i = \omega_0 + \gamma G \cdot r_i, \quad (3)$$

where ω_i is the Larmor frequency of interest, ω_0 is the resident frequency, γ is the gyromagnetic ratio, G is the gradient, and r_i is the direction. For example, application of the gradient in the x direction (usually the read direction) has the following result:

$$\omega_x = \omega_0 + \gamma G \cdot r_x. \quad (4)$$

These changes in the frequency direction are recorded for reconstruction of the image.

Slice-Selection Gradient.—A slice-selection gradient (G_z or G_{SS}) determines the amount of tissue (slice) to be excited by using an RF pulse with a fixed bandwidth that is applied in the presence of a slice-selection gradient. The slice-selection gradient creates a one-to-one correspondence between the bandwidth of the RF pulse and a narrow "slice" of tissue that is to be excited. This RF pulse is called a B_1 field and is applied in the presence of B_0, so that all spins (protons) are at the same resonance frequency and the excitation is nonselective (31,37). The parameters that determine the slice thickness are the bandwidth of the RF pulse (Δf) and the gradient strength across the FOV (G_z), as shown in Figure 3. In general, larger gradients will give thinner slices and smaller gradients will give thicker slices.

Frequency-Encoding or Readout Gradient.—The frequency-encoding gradient (G_x or $G_{readout}$), commonly referred to as the readout gradient, is applied perpendicular to the slice-selection gradient before and during the echo formation (24). The protons are spatially "frequency encoded" by their characteristic resonant frequency along the x axis. The readout gradient is used to frequency encode the spectrum of frequencies from the object that have been created by the presence of the frequency-encoding gradient. Thus, the MR signal is always acquired during the readout gradient (Fig 4).

Phase-Encoding Gradient.—The phase-encoding gradient (G_y or G_{PE}) is applied along the third perpendicular axis after the slice-selection gradient and before the readout gradient (33,34, 36,37,50,51). The phase variations occur after the initial excitation, as they begin to dephase along the applied gradient. The phase gradient induces a linear variation of the phase of the magnetization across the image (31,37). The protons will have different phase depending on where they are located; for example, usually positive phase changes occur with a higher magnetic field, whereas negative phase changes are associated with a weaker magnetic field (Fig 5). Notably,

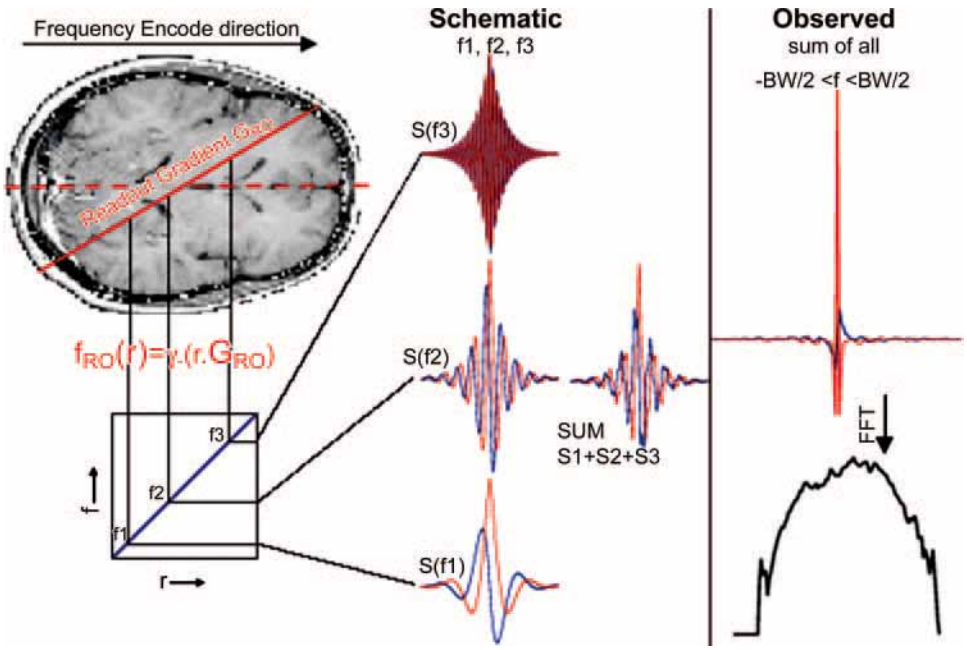


Figure 4. Readout gradient for three discrete frequencies associated with three positions and their summed signal. Also shown are the actual readout signal, which is the sum of signals at all frequencies within the bandwidth *(BW)*, and the fast Fourier transform *(FFT)* of this signal, which is a projection of the object along the frequency-encoding axis.

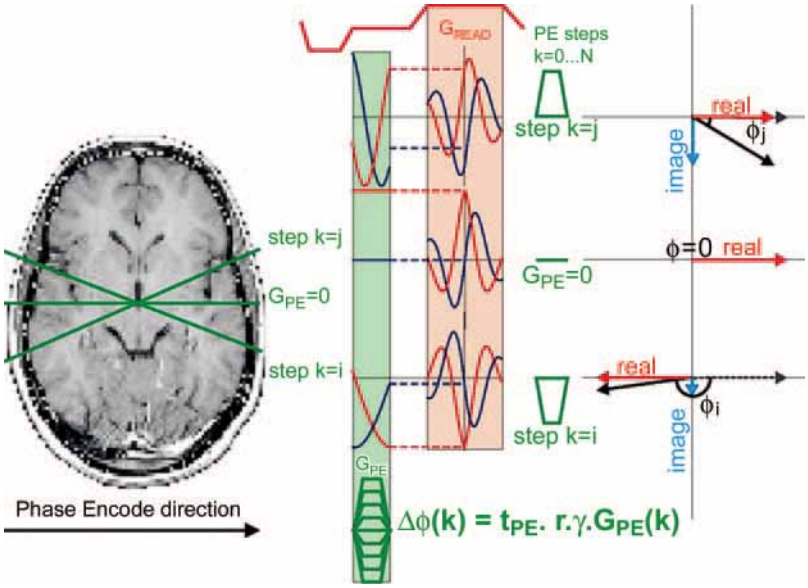


Figure 5. Phase encoding. The readout experiment shown in Figure 4 is repeated N times (N is the desired image resolution) with a short gradient pulse of amplitude $G_{PE}(k)$ and length t_{PE} preceding readout. This gradient pulse temporarily changes the frequency; after period t_{PE}, the result is a phase shift $\Delta(k,r)$. If the gradient pulse amplitude $G_{PE}(k)$ or length is varied in N equal steps, the resulting set of phase-encoded profiles (after the fast Fourier transform of the readout direction) will be the Fourier transform of the object along the phase-encoding direction.

most artifacts occur in the phase direction due to the longer acquisition time of the phase-encoding steps (from about 100 msec to seconds) (52).

By combining the frequency- and phase-encoding gradients, each pixel will have a distinct frequency and phase associated with it. This allows creation of an image of the object by using mathematical methods. By combining all these steps into a pulse sequence, we can generate an MR image (Fig 6).

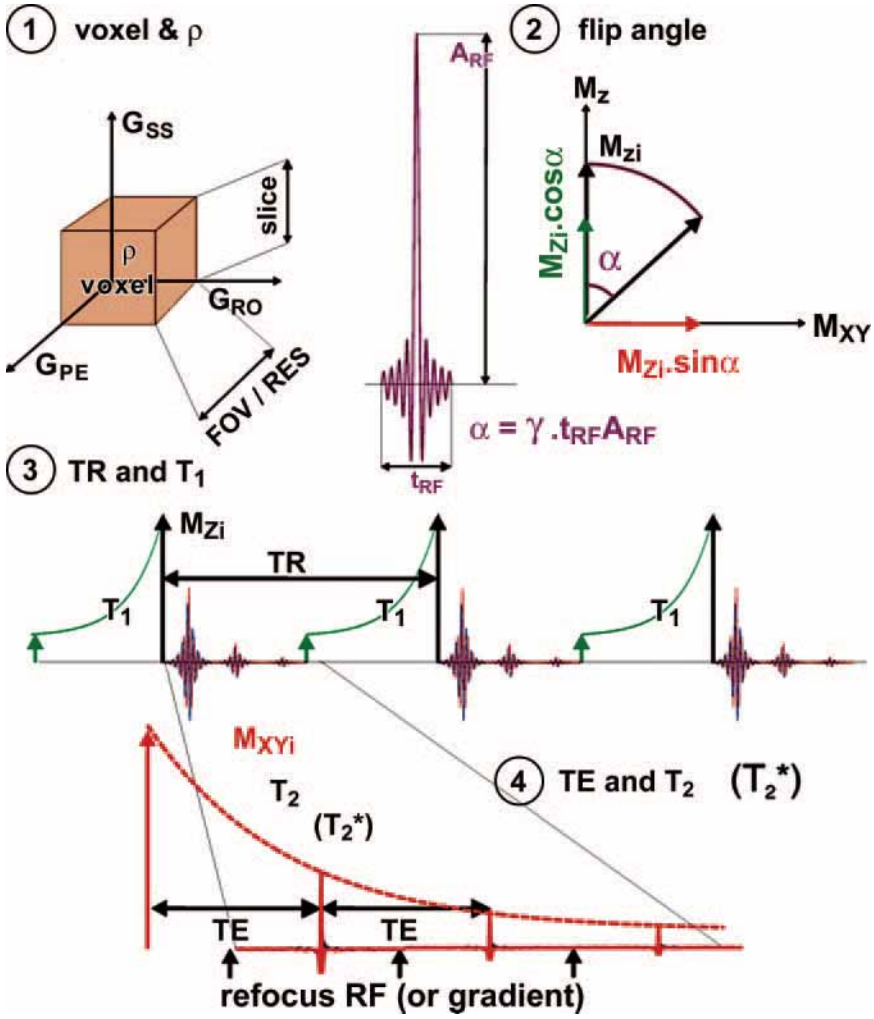


Figure 6. Four basic factors determining the pixel brightness of an MR image. *1*, Application of each gradient for a voxel density (ρ) for localization of the MR signal. *RES* = resolution. *2*, Use of the RF pulse to invert the magnetization signal within the voxel (ρ). Note that α = time of the RF pulse and area covered by the pulse (eg, the strength of the pulse). *M* = magnetization. *3*, Graphic representation of the relaxation parameter T1. *TR* = repetition time. *4*, Graphic representation of the relaxation parameter T2. *TE* = echo time.

MR Signal (T1 and T2)

Teaching Point

The mechanism for contrast in an MR image is governed by the application of an RF pulse and, more important, the relaxation times of the tissue of interest, in particular T1 and T2. After the RF pulse, an MR signal is created. This MR signal is defined by a phenomenological equation called the Bloch equation (53,54). The Bloch equation can be solved for T1 and T2 for a spin-echo sequence:

$$M(t) = M_0(1 - e^{(-t/T1)}) \quad (5)$$

and

$$M_{xy}(t) = M_{xy}e^{(-t/T2)}. \quad (6)$$

From these equations, we can see that MR pixel intensity is proportional to the number of protons within the tissue, T1, and T2. The reader should consult the references for derivation of the Bloch equation; it is beyond the scope of this article.

T1 is the longitudinal relaxation time. This occurs after application of a 180° RF pulse, where the magnetization vector is inverted. Then a recovery process occurs. T1 weighting of the image is dependent on the amount of TR in milliseconds between the slice selection and RF pulses and the field strength. For example, in a spin-echo sequence (23), the TR is the amount of time between two successive 90° pulses, which affects the longitudinal relaxation time. In general, fatty tissue (short T1) is bright on a T1-weighted image, and water (or spinal fluid) is dark (long T1). Tissues that are solid have an intermediate T1 signal and may appear isointense (Fig 7).

Teaching Point

Conversely, T2 is called the transverse relaxation time and pertains to a decay process. T2-weighted images are dependent on the amount of TE in milliseconds. The TE is defined as the time of the echo. This occurs after a short waiting period (TE/2), in which a 180° pulse in a spin echo is applied and an echo is formed. In contrast to T1-weighted images, water is bright (long T2) on

Teaching Point

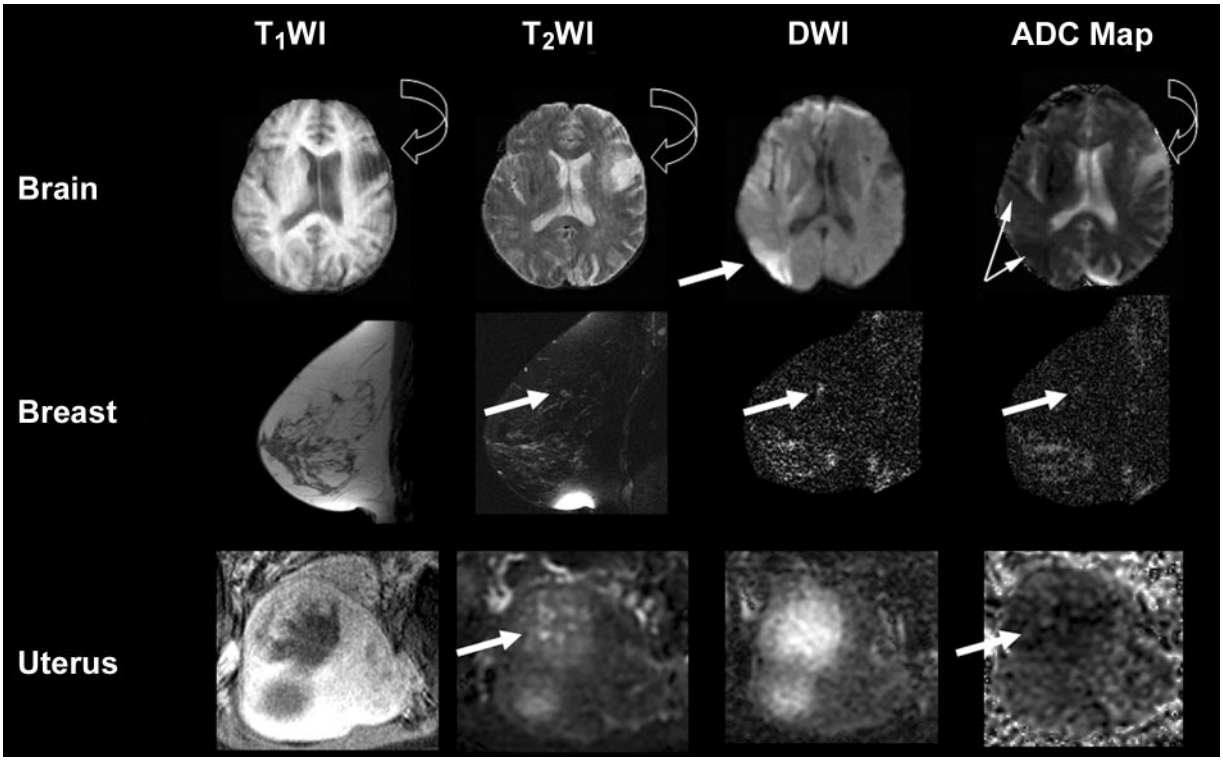


Figure 7. T1-weighted images *(T1WI)*, T2-weighted images *(T2WI)*, and diffusion-weighted images *(DWI)* from different regions of the body with corresponding maps of the apparent diffusion coefficient *(ADC)* of water. Top: Brain images of a patient with an acute stroke (<6 hours) and older infarct (>3 months). The regions of infarction are clearly visualized on the T1- and T2-weighted images as low (T1) and high (T2) signal intensity in the left temporal lobe (open arrow). Conversely, in the right occipital lobe, there is little or no change in the regions of new ischemia, except that they are seen as hyperintense areas on the diffusion-weighted image (single solid arrow). On the ADC map, there are corresponding hypointense regions (double solid arrow), which have lower ADC values. Areas that are hyperintense on the ADC map have higher ADC values. Similar signal intensities are noted on images of the breast (middle) and uterus (bottom). Note the changes (arrow in bottom row) on the diffusion-weighted image of the uterus, with decreased signal intensity in the same regions on the ADC map. Similar changes are seen on the breast images (arrow in middle row). These examples demonstrate the versatility of MR imaging in producing different image contrasts.

T2-weighted images, fatty tissue (intermediate T2) is generally isointense, and tissues that are solid have a short T2 signal and may appear hypointense (depending on the TE). In terms of tissue relaxation times, T1 is greater than T2 for different tissues. In summary, T1-weighted images have a short TR and short TE (eg, 700/20 msec), while T2-weighted images have a long TR and long TE (eg, 2000/80 msec).

Basic MR Sequences

There are two basic MR sequences that are frequently used for MR imaging: spin-echo or gradient-echo techniques (23,55). They differ by the number of RF pulses and the use of gradient reversals to produce an echo. Spin-echo sequences use a 90° RF pulse followed by a 180° RF pulse to generate the spin echo. Conversely, in gradient-echo methods, a single RF pulse (flip angle) is used to invert the longitudinal magnetization, then the gradient changes from negative values and/or to positive values (gradient reversals). These gradient reversals cause phase dispersion followed by rephasing of the spins, which forms an echo (55).

What Is k-Space?

The data obtained from the gradients (read and phase) are stored in a "matrix format" that contains all the pertinent information (eg, localization, frequency, and phase of each pixel location). In this matrix, different locations have varying amounts of signal information that is present in the reconstructed image. For example, in typical objects, high-signal information is concentrated in the center and low-signal information in general is near the peripheral sections (which define the edges). This can be demonstrated by taking

regions of the k-space out and then using mathematical transforms on the "intact" k-space to reconstruct the image (Fig 8). The matrix formation can be viewed in what is termed "k-space formalism" or "reciprocal space" (36,38,51,57,58). Formally, k-space is defined as an array of "complex" data points (k_x and k_y) in multidimensional space (eg, two-dimensional, three-dimensional).

We define the signal equation as follows (33,36,57):

$$s(t) \propto \int \rho(e^{-TE/T2})(1 - e^{-TR/T1}), \qquad (7)$$

where ρ = proton density. Thus, we can image tissue using different tissue contrast–based applications and manipulations of the T1 and T2 characteristics. After application of each gradient (read and phase), we have a matrix of points in k-space or data space. This set of data has units of time and is sometimes referred to as the time domain.

Knowing the relationship between the FOV and gradient direction, we can relate this to the change in k-space as shown below. Recall that FOV is defined as the bandwidth divided by the gradient times the gyromagnetic ratio:

$$\mathrm{FOV} = \frac{\mathrm{BW}}{\gamma G}. \qquad (8)$$

Now we know that the bandwidth is defined as follows:

$$\mathrm{BW} = \frac{1}{\Delta T}, \qquad (9)$$

where ΔT is the sampling rate. Therefore, by combining the two equations, we see the following relationship:

$$\mathrm{FOV} = \frac{\mathrm{BW}}{\gamma G} = \frac{1}{\gamma G \Delta T}. \qquad (10)$$

The units are distance (millimeters or centimeters).

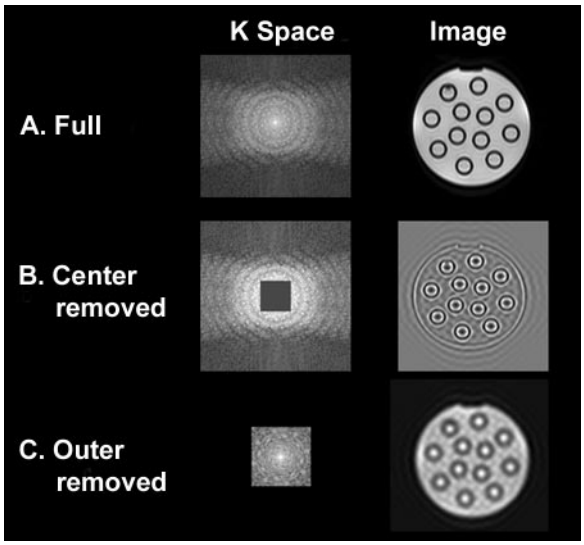


Figure 8. Effects of removing k-space data on a reconstructed phantom image. In *A*, image was obtained with full k-space. In *B*, image obtained with the center of k-space missing shows only edges and fine detail, which are defined by high-frequency k-space. In general, the maximum signal is obtained from the center of k-space. In *C*, image obtained with only the outer portion of central k-space removed is blurred and lacks detail. In *B* and *C*, note that removal of portions of k-space leads to ringing artifacts in the image (56).

Now we can define the following relationship:

$$\Delta k = \gamma G_i \Delta t_i;\ i = x,y. \qquad (11)$$

Thus, there is a direct correspondence between the FOV and gradient direction. We can relate this to the change in k-space as follows:

$$\mathrm{FOV} = \frac{1}{\gamma G \Delta T} \Rightarrow \gamma G \Delta T = \frac{1}{\mathrm{FOV}}$$

$$\Rightarrow \Delta k = \frac{1}{\mathrm{FOV}}. \qquad (12)$$

The units of Δk are cycles per distance and are called the spatial frequency. Therefore, changes in the FOV are inversely proportional to the spatial frequency of k-space (38).

The traversal of k-space is dependent on the amplitude and timing of the gradients during an MR acquisition. By using mathematical operations, we can transform k-space (spatial frequency domain) into the image domain and create an image. Thus, we can define a practical use for the

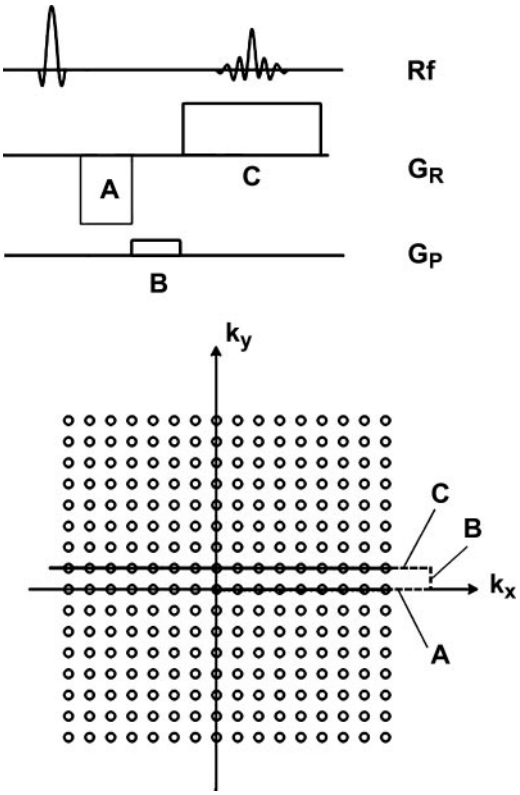


Figure 9. Path through k-space of a gradient-echo sequence with phase encoding. Sequence diagram shows the excitation pulse and signals RF, the readout gradient G_R, and the phase-encoding gradient G_P. The prewinding gradient *A* carries the k-space trajectory in the k_x direction out of the sampling area. Phase encoding with *B* causes an offset of the trajectory in the k_y direction, where signal from one k-line is read out under *C*. Data are acquired only during the last part (solid line in the trajectory), and signal during *A* and *B* is discarded (dashed line). The experiment is repeated with different *B* until all k-lines have been acquired (58).

k-space equation in terms of the gradients (read and phase) used in MR imaging as follows (36,38):

$$k_y = \gamma(G_{\text{phase encode}} \cdot t_{\text{phase encode}}) \qquad (13)$$

and

$$k_x = \gamma(G_{\text{readout}} \cdot t_{\text{readout}}), \qquad (14)$$

where t_{phase} or t_{read} is the cumulative time for each gradient (36).

Basically, for a gradient-echo sequence, after the image sequence is executed, the regions of k-space are filled and details of certain features within the image can be visualized. The phase gradient moves the k-space vector through the trajectory from a starting point (0,0). Then, the read gradient transverses the region of k-space during the signal acquisition (eg, right to left, circular) in the k_x direction, whereas the phase gradient moves the k_y. These movements in k-space are collected into a data matrix, then a mathematical Fourier transform is applied to the data matrix to form an image (Fig 9) (31,57). Because of this knowledge, k-space acquisitions can be tailored for quicker acquisition by relying on the periodic nature of k-space, such as partial k-space acquisitions. These regions in k-space have specific properties: for example, in the typical object, the center of k-space determines much of the contrast in the image, whereas the outer regions of k-space determine capacity to image sharp edges and determine image resolution. By removing portions of the data, changes in the image can be seen (Fig 8).

This type of information is useful when looking for artifacts. Artifacts are caused by changes in the phase of the signal during the phase-encoding gradient (57,58), typically seen in areas of flow, motion, B_0 inhomogeneities, and chemical shift of protons (eg, fat and water). More detailed information about k-space can be found in references 38, 51, 57, and 58.

Parallel Imaging

Parallel imaging is a relatively new area of MR imaging and is quickly becoming a routinely used tool for decreasing imaging times in the clinical setting (59). Parallel imaging methods are based on the deployment of several RF coils (phased array) to "speed up" the acquisition of the MR signal, that is, to reduce the number of phase-encoding steps, because the imaging time required for each acquisition is proportional to the number of phase-encoding steps. The acceleration or reduction factor is called *R* and is usually set at 2 or 3, but this also reduces the FOV in the phase direction and leads to aliasing of the object, which is corrected by using B_1 coil sensitivity maps. This concept was suggested by Hutchinson and Raff (60) and later by other investigators (61,62).

Sodickson and Manning (47) introduced parallel imaging into practice by using simultaneous acquisition of spatial harmonics (SMASH). Briefly, SMASH acquires a reduced set (determined by the *R* factor) of phase encodes in k-space. The *R* factor is defined as increasing the distance between lines of k_y with the spatial resolution at a fixed number. This leads to a reduction in imaging time. *R* is also known as the acceleration factor, and typical factors used are 2–3. But, with a reduction in the number of phase-encoding lines, there is a decrease in the FOV, which leads to "wraparound" or aliasing of the object. Then, B_1 coil sensitivity profiles are generated and basis sets are used to approximate the missing phase-encoding lines before application of the Fourier transform to obtain an unaliased image. This requires linear combinations of B_1 coil sensitivity profiles to obtain the spatial harmonics.

In contrast, Pruessmann et al (48) introduced sensitivity encoding (SENSE) as an alternative approach for SMASH parallel imaging. In SENSE imaging, the B_1 sensitivity profiles of each coil are used to "unwrap" the image after the Fourier transform, and this is performed in the image domain. However, there is an SNR cost with the reduction of imaging time, that is, lower SNR in the image. In SENSE imaging, this reduction of SNR is about the square root of *R* and is called the geometry factor, *g*, which represents the noise magnification after unwrapping (37,48).

The reader is referred to the references for more in-depth detail about each method (37, 47,48). Applications of these methods are currently increasing due to improved and greater numbers of channels in the RF coils (63). This will lead to a reduction of imaging time (37) and reduced artifacts in echo-planar imaging (64) and is an active area of research.

Contrast Mechanisms and MR Imaging Parameters

The contrast between different tissues in the MR image is defined by a complex interaction between several user-defined and tissue-of-interest variables; these are commonly referred to as intrinsic and extrinsic variables (29,33,34,36,39). The SNR is a major determinant of whether there is sufficient signal to differentiate between different tissue types. SNRs are calculated by using the following equation:

$$\text{SNR} \propto (\text{volume})\sqrt{\frac{\#\text{PE} \cdot \text{NEX}}{\text{BW}}}, \qquad (15)$$

where PE is the number of phase-encoding steps, NEX is the number of signals acquired, and BW is the bandwidth (29,39,65,66).

The signal intensity depends on several parameters that are basic to any MR sequence. For example, some MR parameters are TE, TR, flip angle (α)—the angle to rotate (or tip) the magnetization vector from the main B_0 field onto the transverse plane (5°–90°)—slice thickness, and FOV (33,34,36). The amount of TR and TE determines the amount of T1 or T2 weighting for the images, respectively, whereas the slice thickness governs the amount of protons available in the tissue to image; for example, larger slices have better SNR than thinner slices but have increased partial volume effects (33,34,36). For instance, in spin-echo sequences, T1-weighted images usually have short TR (to maximize T1 differences in tissue) and short TE (to minimize T2 effects), whereas T2-weighted sequences have long TR (1500 msec) and TE (>80 msec). Therefore, the investigator can change the MR parameters (eg, TR, TE) as needed for the desired application (29,39).

Selected Applications

Teaching Point

The real power of MR imaging lies in the wide range of applications for which it can be used. Current applications include soft-tissue delineation, determining extent of disease, tumor staging, functional and metabolic information, and monitoring response to treatment. Some of these newer applications are outlined herein.

T1- and T2-weighted Imaging

T1- and T2-weighted imaging are the most widely used sequences for soft-tissue delineation of anatomic structures and related pathologic conditions (Fig 7). For example, in the brain, T2- and T1-weighted imaging with or without contrast material can be used to see changes in white or gray matter. In other body organs, such as the breast, extremities, and liver, and in uterine lesions, imaging has been performed by using combinations of modalities such as ultrasonography and/or T2- and T1-weighted MR imaging.

Diffusion-weighted and Perfusion-weighted Imaging

Diffusion-weighted imaging (DWI) and perfusion-weighted imaging (PWI) are used in neurologic applications, such as brain tumor imaging (67–69) and cerebral ischemia (70–72). The use of perfusion and diffusion MR imaging techniques can identify regions of abnormal brain tissue after cerebral ischemia. PWI readily depicts areas of brain with a compromised cerebral blood

flow, whereas DWI can depict regions of ischemic tissue that may or may not recover, depending on the duration of reduced blood flow (73,74). By combining PWI and DWI methods, three scenarios can be observed: PWI > DWI (mismatch), PWI = DWI (match), or DWI > PWI (reverse mismatch) (75). For example, if PWI is larger than DWI, then the area depicted may represent "at risk" or penumbral tissue (76–78). Evaluation of these tissue characteristics is important for the targeting of therapeutic measures to maximize clinical outcomes.

DWI has been used in other organs of the body, for example, in the liver for demonstration of metastatic disease and response to treatment (79), in the uterus for monitoring treatment response from interventional procedures such as uterine arterial embolization (80) and high-intensity focused ultrasound surgery (81), and for classification of breast lesions (82). Still larger studies are needed to fully understand the impact that DWI will have in these applications.

Spectroscopy

Proton spectroscopy has been used primarily for brain applications and recently for other organs, such as the liver, breast, prostate, and soft tissue. The use of spectroscopy expands the repertoire of clinical information by providing information on intracellular metabolites, such as choline (3.2 ppm), creatine (3.0 ppm), citrate (2.6 ppm), *N*-acetyl aspartate (2.02 ppm), and lactate (1.4 ppm) (6,7,83–85). (The unit "ppm" is defined as "parts per million" and is independent of the strength of the imaging unit.)

These metabolites are known to change in different pathologic conditions; for example, in brain tumors, *N*-acetyl aspartate (2.02 ppm) decreases with a subsequent increase in choline (6,7,85). In the breast, the presence of a choline peak (3.2 ppm) is suggestive of malignancy (11,12,86,87). In the prostate, MR spectroscopy is being increasingly used in conjunction with MR imaging to provide information on the presence or absence of citrate (2.6 ppm) and/or choline (3.2 ppm) (14,88). These applications will become routine procedures in the near future (89).

^{23}Na (Sodium) MR Imaging

Sodium is abundant in most tissues and is actively pumped out of healthy cells by the Na^+/H^+-ATPase pump, which maintains a large concentration difference across the cell membrane at the cost of energy-rich adenosine triphosphate. Thus, an increase in intracellular sodium concentration can be a good indicator of compromised cellular membrane integrity or impaired energy metabolism. In the presence of tissue perfusion, the intracellular changes and concurrent increase in vascular or interstitial volume appear to be an equally good indicator of cellular membrane integrity and energy metabolism.

The intracellular sodium cannot be imaged separately from the extracellular sodium concentration without toxic shift reagents or special MR methods that cause a significant reduction in SNR and resolution (90,91). However, the total sodium concentration in tissue can be resolved by using MR imaging, and there has been increased interest in the application of sodium MR (92–98). In particular, sodium imaging has been performed in the brain (93,99), breast (95,98), heart (100), kidney (101), and uterus (102). In recent reports, sodium MR imaging has shown promise in monitoring therapeutic response (96,97,103).

Beyond 3 T: Emerging High-Field-Strength MR Imaging (7 T and Greater)

Although there have been vast technological advances in MR imaging over the past 40 years, the central principle for advancing MR imaging technology has been based on finding ways to increase SNR (40,41) in the MR image. The most fundamental approach to increasing SNR has been to increase the field strength of the MR imaging magnets. As a result, the impetus for improved MR imaging has driven progressive increases in its magnetic field strengths from fractions of a tesla to fields of 1.5 T in the 1980s then to fields of 3 T by the mid-1990s. The next push for increasing MR imaging field strength was possible with the advancement of superconducting technology (104–106). In the late 1990s and early 2000s, the development of a human MR imaging unit above 4.1 T (17), in this case 8 T (44,107, 108), was achieved.

As a result of its tremendous potential (see Fig 2b), human MR imaging is currently performed at field strengths reaching 7 T (21,43), 8 T (44,107,108), and 9.4 T (46). The three major MR imaging vendors—GE Healthcare, Siemens Medical Solutions, and Philips Medical Systems—are developing 7-T whole-body human imaging units. However, as with many scientific breakthroughs, the potential of ultrahigh-field-strength imaging can be achieved only if other challenges are overcome. The most significant of these challenges include *(a)* safety concerns regarding exceeding RF power deposition (109, 110) in tissue and *(b)* noninherent inhomogeneity of MR imaging signal detection across the human head (22,49,108,111–113).

Conclusions

MR imaging provides a powerful tool for diagnosis and excellent soft-tissue contrast because the image contrast can be finely optimized for specific clinical questions. Moreover, novel pulse sequence techniques allow image contrast to be based on tissue physiology or even cellular metabolism in a noninvasive manner. In addition, with ever-increasing improvement in both hardware and software, MR imaging may one day be used for screening of different pathologic conditions and provide a window into cellular metabolism and tissue physiology.

Acknowledgments: We thank the reviewers for their excellent comments and suggestions for this article and Mahadevappa Mahesh, MS, PhD, for his contribution.

References

1. Evelhoch JL. Key factors in the acquisition of contrast kinetic data for oncology. J Magn Reson Imaging 1999;10(3):254–259.
2. Engelbrecht MR, Huisman HJ, Laheij RJ, et al. Discrimination of prostate cancer from normal peripheral zone and central gland tissue by using dynamic contrast-enhanced MR imaging. Radiology 2003;229(1):248–254.
3. Felix R, Schorner W, Laniado M, et al. Brain tumors: MR imaging with gadolinium-DTPA. Radiology 1985;156(3):681–688.
4. Nelson SJ, Huhn S, Vigneron DB, et al. Volume MRI and MRSI techniques for the quantitation of treatment response in brain tumors: presentation of a detailed case study. J Magn Reson Imaging 1997;7(6):1146–1152.
5. Nelson SJ. Analysis of volume MRI and MR spectroscopic imaging data for the evaluation of patients with brain tumors. Magn Reson Med 2001;46(2):228–239.
6. Pouwels PJ, Frahm J. Regional metabolite concentrations in human brain as determined by quantitative localized proton MRS. Magn Reson Med 1998;39(1):53–60.
7. Ross B, Michaelis T. Clinical applications of magnetic resonance spectroscopy. Magn Reson Q 1994;10(4):191–247.
8. Heywang SH, Hahn D, Schmidt H, et al. MR imaging of the breast using gadolinium-DTPA. J Comput Assist Tomogr 1986;10(2):199–204.
9. Kaiser WA, Zeitler E. MR imaging of the breast: fast imaging sequences with and without Gd-DTPA—preliminary observations. Radiology 1989;170(3 pt 1):681–686.
10. Kuhl CK, Mielcareck P, Klaschik S, et al. Dynamic breast MR imaging: are signal intensity time course data useful for differential diagnosis of enhancing lesions? Radiology 1999;211(1):101–110.
11. Roebuck JR, Cecil KM, Schnall MD, Lenkinski RE. Human breast lesions: characterization with proton MR spectroscopy. Radiology 1998;209(1):269–275.
12. Jacobs MA, Barker PB, Bottomley PA, Bhujwalla Z, Bluemke DB. Proton MR spectroscopic imaging of human breast cancer: a preliminary study. J Magn Reson Imaging 2004;19(1):68–75.
13. Macura KJ, Ouwerkerk R, Jacobs MA, Bluemke DA. Patterns of enhancement on breast MR images: interpretation and imaging pitfalls. RadioGraphics 2006;26(6):1719–1734; quiz 1719.
14. Kurhanewicz J, Vigneron DB, Hricak H, Narayan P, Carroll P, Nelson SJ. Three-dimensional H-1 MR spectroscopic imaging of the in situ human prostate with high (0.24–0.7-cm^3) spatial resolution. Radiology 1996;198(3):795–805.
15. Narayan P, Kurhanewicz J. Magnetic resonance spectroscopy in prostate disease: diagnostic possibilities and future developments. Prostate Suppl 1992;4:43–50.
16. Gillies RJ, Bhujwalla ZM, Evelhoch J, et al. Applications of magnetic resonance in model systems: tumor biology and physiology. Neoplasia 2000;2:139–151.
17. Bomsdorf H, Helzel T, Kunz D, Roschmann P, Tschendel O, Wieland J. Spectroscopy and imaging with a 4 tesla whole-body MR system. NMR Biomed 1988;1(3):151–158.
18. Roschmann P. Radiofrequency penetration and absorption in the human body: limitations to high-field whole-body nuclear magnetic resonance imaging. Med Phys 1987;14(6):922–931.
19. Adler DD, Wahl RL. New methods for imaging the breast: techniques, findings, and potential. AJR Am J Roentgenol 1995;164(1):19–30.
20. Robitaille PM, Abduljalil AM, Kangarlu A. Ultra high resolution imaging of the human head at 8 tesla: 2K × 2K for Y2K. J Comput Assist Tomogr 2000;24(1):2–8.
21. Wald LL, Wiggins GC, Potthast A, Wiggins CJ, Triantafyllou C. Design considerations and coil comparisons for 7 T brain imaging. Appl Magn Reson 2005;29(1):19–37.
22. Ibrahim TS, Abraham R, Abraham D, Tang L. RF systems for high-field MRI: problems and possible solutions based on computational electromagnetics. Meeting of the Institute of Electrical and Electronics Engineers, San Francisco, Calif, 2006; 5–8.
23. Hahn EL. Spin echoes. Phys Rev 1950;80(4):580.
24. Lauterbur PC. Image formation by induced local interactions: examples employing nuclear magnetic resonance. Nature 1973;242:190–191.
25. Mansfield P. Multi-planar image formation using NMR spin echoes. J Phys C Solid State 1977;10:L55–L58.
26. Bottomley PA, Andrew ER. RF magnetic field penetration, phase shift and power dissipation in biological tissue: implications for NMR imaging. Phys Med Biol 1978;23(4):630–643.
27. Mansfield P, Morris P; Waugh J, ed. NMR imaging in biomedicine. Cambridge, Mass: Academic Press, 1982.
28. Bottomley PA, Hart HR, Edelstein WA, et al. NMR imaging/spectroscopy system to study both anatomy and metabolism. Lancet 1983;2(8344):273–274.

29. Bottomley PA, Foster TH, Argersinger RE, Pfeifer LM. A review of normal tissue hydrogen NMR relaxation times and relaxation mechanisms from 1–100 MHz: dependence on tissue type, NMR frequency, temperature, species, excision, and age. Med Phys 1984;11(4):425–448.
30. Slichter C. Principles of magnetic resonance. New York, NY: Springer-Verlag, 1990.
31. Nishimura DG. Principles of magnetic resonance imaging [the white book]. D. G. Nishimura, 1996.
32. Vlaardingerbroek M, den Boer J. Magnetic resonance imaging. Berlin, Germany: Springer-Verlag Telos, 1999.
33. Haacke M, Brown R, Thompson M, Venkatesan R. Magnetic resonance imaging: physical principles and sequence design. New York, NY: Wiley-Liss, 1999.
34. Bushberg J, Seibert A, Leidholdt E, Boone J. Essential physics of medical imaging. Philadelphia, Pa: Lippincott Williams & Wilkins, 2002.
35. Hendee WR, Ritenour ER. Medical imaging physics. New York, NY: Wiley-Liss, 2002.
36. Brown MA, Semelka RC. MRI: basic principles and applications. 3rd ed. New York, NY: Wiley-Liss, 2003.
37. Bernstein MA, King KF, Zhou XJ. Handbook of MRI pulse sequences. Burlington, Mass: Elsevier Academic Press, 2004.
38. Hashemi RH, Bradley WG, Lisanti CJ. MRI: the basics. Philadelphia, Pa: Lippincott Williams & Wilkins, 2004.
39. Edelstein WA, Bottomley PA, Hart HR, Smith LS. Signal, noise, and contrast in nuclear magnetic resonance (NMR) imaging. J Comput Assist Tomogr 1983;7(3):391–401.
40. Hoult DI, Lauterbur PC. The sensitivity of the zeugmatographic experiment involving human samples. J Magn Reson 1979;34(2):425–433.
41. Hoult DI, Richards RE. The signal-to-noise ratio of the nuclear magnetic resonance experiment. J Magn Reson 1976;24(1):71–85.
42. Gillies R. NMR in physiology and biomedicine. New York, NY: Academic Press, 1994.
43. Vaughan JT, Garwood M, Collins CM, et al. 7T vs. 4T: RF power, homogeneity, and signal-to-noise comparison in head images. Magn Reson Med 2001;46(1):24–30.
44. Robitaille PM, Abduljalil AM, Kangarlu A, et al. Human magnetic resonance imaging at 8 T. NMR Biomed 1998;11(6):263–265.
45. Ibrahim TS, Kangarlu A, Chakeress DW. Design and performance issues of RF coils utilized in ultra high field MRI: experimental and numerical evaluations. IEEE Trans Biomed Eng 2005; 52(7):1278–1284.
46. Vaughan JT. How to do RF at high fields. Presented at the annual meeting of the International Society for Magnetic Resonance in Medicine, Miami, Fla, 2005.
47. Sodickson DK, Manning WJ. Simultaneous acquisition of spatial harmonics (SMASH): fast imaging with radiofrequency coil arrays. Magn Reson Med 1997;38(4):591–603.
48. Pruessmann KP, Weiger M, Scheidegger MB, Boesiger P. SENSE: sensitivity encoding for fast MRI. Magn Reson Med 1999;42(5):952–962.
49. Ibrahim TS, Mitchell C, Schmalbrock P, Lee R, Chakeres DW. Electromagnetic perspective on the operation of RF coils at 1.5–11.7 tesla. Magn Reson Med 2005;54(3):683–690.
50. Kumar A, Welti D, Ernst R. NMR Fourier zeugmatography. J Magn Reson 1975;18:69–83.
51. Edelstein WA, Hutchison JM, Johnson G, Redpath T. Spin warp NMR imaging and applications to human whole-body imaging. Phys Med Biol 1980;25(4):751–756.
52. Elster A, Burdette J. Questions and answers in magnetic resonance imaging. St Louis, Mo: Mosby–Year Book, 2001.
53. Bloch F, Hansen W, Packard M. The nuclear induction experiment. Phys Rev 1946;70:474–485.
54. Bloch F. Nuclear induction. Phys Rev 1946;70: 460–474.
55. Frahm J, Haase A, Matthaei D. Rapid three-dimensional MR imaging using the FLASH technique. J Comput Assist Tomogr 1986;10(2): 363–368.
56. Higgins DM. ReviseMRI.com. Available at: http://www.revisemri.com.
57. Twieg DB. The k-trajectory formulation of the NMR imaging process with applications in analysis and synthesis of imaging methods. Med Phys 1983;10(5):610–621.
58. Hennig J. K-space sampling strategies. Eur Radiol 1999;9(6):1020–1031.
59. Glockner JF, Hu HH, Stanley DW, Angelos L, King K. Parallel MR imaging: a user's guide. RadioGraphics 2005;25(5):1279–1297.
60. Hutchinson M, Raff U. Fast MRI data acquisition using multiple detectors. Magn Reson Med 1988;6(1):87–91.
61. Kwiat D, Einav S, Navon G. A decoupled coil detector array for fast image acquisition in magnetic resonance imaging. Med Phys 1991;18(2): 251–265.
62. Ra JB, Rim CY. Fast imaging using subencoding data sets from multiple detectors. Magn Reson Med 1993;30(1):142–145.
63. van den Brink JS, Watanabe Y, Kuhl CK, et al. Implications of SENSE MR in routine clinical practice. Eur J Radiol 2003;46(1):3–27.
64. Bammer R, Auer M, Keeling SL, et al. Diffusion tensor imaging using single-shot SENSE-EPI. Magn Reson Med 2002;48(1):128–136.
65. Hendrick RE, Nelson TR, Hendee WR. Optimizing tissue contrast in magnetic resonance imaging. Magn Reson Imaging 1984;2(3):193–204.
66. Lee JN, Riederer SJ. The contrast-to-noise in relaxation time, synthetic, and weighted-sum MR images. Magn Reson Med 1987;5(1):13–22.
67. Chenevert TL, McKeever PE, Ross BD. Monitoring early response of experimental brain tumors to therapy using diffusion magnetic resonance imaging. Clin Cancer Res 1997;3(9): 1457–1466.
68. Chenevert TL, Stegman LD, Taylor JM, et al. Diffusion magnetic resonance imaging: an early surrogate marker of therapeutic efficacy in brain tumors. J Natl Cancer Inst 2000;92(24):2029–2036.

69. Pomper MG, Port JD. New techniques in MR imaging of brain tumors. Magn Reson Imaging Clin N Am 2000;8(4):691–713.
70. Le Bihan D, Breton E, Lallemand D, Grenier P, Cabanis E, Laval Jeantet M. MR imaging of intravoxel incoherent motions: application to diffusion and perfusion in neurologic disorders. Radiology 1986;161:401–407.
71. Moseley ME, Kucharczyk J, Mintorovitch J, et al. Diffusion-weighted MR imaging of acute stroke: correlation with T2-weighted and magnetic susceptibility–enhanced MR imaging in cats. AJNR Am J Neuroradiol 1990;11(3):423–429.
72. Warach S, Chien D, Li W, Ronthal M, Edelman RR. Fast magnetic resonance diffusion-weighted imaging of acute human stroke. Neurology 1992; 42:1717–1723.
73. Kidwell CS, Saver JL, Mattiello J, et al. Thrombolytic reversal of acute human cerebral ischemic injury shown by diffusion/perfusion magnetic resonance imaging. Ann Neurol 2000;47(4):462–469.
74. Rivers CS, Wardlaw JM, Armitage PA, et al. Do acute diffusion- and perfusion-weighted MRI lesions identify final infarct volume in ischemic stroke? Stroke 2006;37(1):98–104.
75. Restrepo L, Jacobs MA, Barker PB, et al. Etiology of perfusion-diffusion magnetic resonance imaging mismatch patterns. J Neuroimaging 2005;15(3):254–260.
76. Sorensen AG, Buonanno FS, Gonzalez RG, et al. Hyperacute stroke: evaluation with combined multisection diffusion-weighted and hemodynamically weighted echo-planar MR imaging. Radiology 1996;199(2):391–401.
77. Neumann-Haefelin T, Wittsack HJ, Wenserski F, et al. Diffusion- and perfusion-weighted MRI: the DWI/PWI mismatch region in acute stroke. Stroke 1999;30(8):1591–1597.
78. Kidwell CS, Alger JR, Saver JL. Beyond mismatch: evolving paradigms in imaging the ischemic penumbra with multimodal magnetic resonance imaging. Stroke 2003;34(11):2729–2735.
79. Kamel IR, Bluemke DA, Eng J, et al. The role of functional MR imaging in the assessment of tumor response after chemoembolization in patients with hepatocellular carcinoma. J Vasc Interv Radiol 2006;17(3):505–512.
80. Liapi E, Kamel IR, Bluemke DA, Jacobs MA, Kim HS. Assessment of response of uterine fibroids and myometrium to embolization using diffusion-weighted echoplanar MR imaging. J Comput Assist Tomogr 2005;29(1):83–86.
81. Jacobs MA, Herskovits EH, Kim HS. Uterine fibroids: diffusion-weighted MR imaging for monitoring therapy with focused ultrasound surgery—preliminary study. Radiology 2005;236(1): 196–203.
82. Guo Y, Cai YQ, Cai ZL, et al. Differentiation of clinically benign and malignant breast lesions using diffusion-weighted imaging. J Magn Reson Imaging 2002;16(2):172–178.
83. Duyn JH, Gillen J, Sobering G, van Zijl PC, Moonen CT. Multisection proton MR spectroscopic imaging of the brain. Radiology 1993; 188(1):277–282.
84. Henriksen O. In vivo quantitation of metabolite concentrations in the brain by means of proton MRS. NMR Biomed 1995;8(4):139–148.
85. Barker PB, Glickson JD, Bryan RN. In vivo magnetic resonance spectroscopy of human brain tumors. Top Magn Reson Imaging 1993;5(1):32–45.
86. Yeung DK, Cheung HS, Tse GM. Human breast lesions: characterization with contrast-enhanced in vivo proton MR spectroscopy—initial results. Radiology 2001;220(1):40–46.
87. Meisamy S, Bolan PJ, Baker EH, et al. Neoadjuvant chemotherapy of locally advanced breast cancer: predicting response with in vivo ^{1}H MR spectroscopy—a pilot study at 4 T. Radiology 2004;233(2):424–431.
88. Kurhanewicz J, Vigneron DB, Nelson SJ, et al. Citrate as an in vivo marker to discriminate prostate cancer from benign prostatic hyperplasia and normal prostate peripheral zone: detection via localized proton spectroscopy. Urology 1995; 45(3):459–466.
89. Glunde K, Jacobs MA, Bhujwalla ZM. Choline metabolism in cancer: implications for diagnosis and therapy. Expert Rev Mol Diagn 2006;6(6): 821–829.
90. Winter PM, Bansal N. $TmDOTP^{5-}$ as a ^{23}Na shift reagent for the subcutaneously implanted 9L gliosarcoma in rats. Magn Reson Med 2001; 45(3):436–442.
91. Winter PM, Bansal N. Triple-quantum-filtered ^{23}Na NMR spectroscopy of subcutaneously implanted 9L gliosarcoma in the rat in the presence of $TmDOTP^{5-}$. J Magn Reson 2001;152(1):70–78.
92. Perman WH, Thomasson DM, Bernstein MA, Turski PA. Multiple short-echo (2.5-ms) quantitation of in vivo sodium T2 relaxation. Magn Reson Med 1989;9(2):153–160.
93. Thulborn KR, Gindin TS, Davis D, Erb P. Comprehensive MR imaging protocol for stroke management: tissue sodium concentration as a

measure of tissue viability in nonhuman primate studies and in clinical studies. Radiology 1999; 213(1):156–166.
94. Ouwerkerk R, Jacobs MA, Bottomley PA, Fajardo LL. A method for quantifying tissue sodium in breast tumors with short echo time ^{23}Na MRI [abstr]. In: Proceedings of the 10th Meeting of the International Society for Magnetic Resonance in Medicine. Berkeley, Calif: International Society for Magnetic Resonance in Medicine, 2002; 2060.
95. Jacobs MA, Ouwerkerk R, Wolff AC, et al. Multiparametric and multinuclear magnetic resonance imaging of human breast cancer: current applications. Technol Cancer Res Treat 2004; 3(6):543–550.
96. Schepkin VD, Ross BD, Chenevert TL, et al. Sodium magnetic resonance imaging of chemotherapeutic response in a rat glioma. Magn Reson Med 2005;53(1):85–92.
97. Schepkin VD, Lee KC, Kuszpit K, et al. Proton and sodium MRI assessment of emerging tumor chemotherapeutic resistance. NMR Biomed 2006;19(8):1035–1042.
98. Ouwerkerk R, Jacobs MA, Macura KJ, et al. Elevated tissue sodium concentration in malignant breast lesions detected with non-invasive (23)Na MRI. Breast Cancer Res Treat 2007 Jan 27; [Epub ahead of print].
99. Ouwerkerk R, Bleich KB, Gillen JS, Pomper MG, Bottomley PA. Tissue sodium concentration in human brain tumors as measured with ^{23}Na MR imaging. Radiology 2003;227(2):529–537.
100. Ouwerkerk R, Weiss RG, Bottomley PA. Measuring human cardiac tissue sodium concentrations using surface coils, adiabatic excitation, and twisted projection imaging with minimal T2 losses. J Magn Reson Imaging 2005;21(5):546–555.
101. Maril N, Rosen Y, Reynolds GH, Ivanishev A, Ngo L, Lenkinski RE. Sodium MRI of the human kidney at 3 tesla. Magn Reson Med 2006; 56(6):1229–1234.
102. Jacobs MA, Ouwerkerk R, Bottomley PA, Kim HS. Multiparametric proton and sodium MRI of uterine fibroids pre- and post-treatment [abstr]. In: Proceedings of the 13th Meeting of the International Society for Magnetic Resonance in Medicine. Berkeley, Calif: International Society for Magnetic Resonance in Medicine, 2005; 13.
103. Jacobs MA, Ouwerkerk R, Bottomley PA, et al. Multiparameter proton, sodium, and spectroscopic imaging of human breast cancer [abstr]. In: Proceedings of the 11th Meeting of the International Society for Magnetic Resonance in Medicine. Berkeley, Calif: International Society for Magnetic Resonance in Medicine, 2003.
104. Rosner CH, Markiewicz WD. High-field superconducting tape magnet technology. IEEE Trans Magn 1992;28(1):782–786.
105. Heussner RW, Nunes CB, Lee PJ, Larbalestier DC, Jablonski PD. Properties of niobium-titanium superconducting wires with Nb artificial pinning centers. J Appl Phys 1996;80(3):1640–1646.
106. Rudziak MK, Seuntjens JM, Renaud CV, Wong T, Wong J. Development of Apc Nb-Ti composite conductors at Supercon, Inc. IEEE Trans Appl Superconductivity 1995;5(2):1709–1712.
107. Kangarlu A, Baertlein BA, Lee R, et al. Dielectric resonance phenomena in ultra high field MRI. J Comput Assist Tomogr 1999;23(6):821–831.
108. Ibrahim TS, Lee R, Abduljalil AM, Baertlein BA, Robitaille PM. Dielectric resonances and B(1) field inhomogeneity in UHFMRI: computational analysis and experimental findings. Magn Reson Imaging 2001;19(2):219–226.
109. Chen CN, Sank VJ, Cohen SM, Hoult DI. The field dependence of NMR imaging. I. Laboratory assessment of signal-to-noise ratio and power deposition. Magn Reson Med 1986;3(5):722–729.
110. Ibrahim TS. A numerical analysis of radio-frequency power requirements in magnetic resonance imaging experiment. IEEE Trans Microw Theory Tech 2004;52(8):1999–2003.
111. Ibrahim TS, Lee R, Baertlein BA, Abduljalil AM, Zhu H, Robitaille PM. Effect of RF coil excitation on field inhomogeneity at ultra high fields: a field optimized TEM resonator. Magn Reson Imaging 2001;19(10):1339–1347.
112. Beck BL, Jenkins K, Caserta J, Padgett K, Fitzsimmons J, Blackband SJ. Observation of significant signal voids in images of large biological samples at 11.1 T. Magn Reson Med 2004; 51(6):1103–1107.
113. Liu F, Beck BL, Xu B, Fitzsimmons JR, Blackband SJ, Crozier S. Numerical modeling of 11.1T MRI of a human head using a MoM/FDTD method. Concepts Magn Reson B Magn Reson Eng 2005;24B(1):28–38.

Teaching Points

Page 23

Localization of the MR signal is obtained by applying a gradient that produces a controlled linear spatial variation of the B0 magnetic field (z direction), which creates small perturbations to the field in three directions (x, y, and z) (Fig 1).

Page 26

The mechanism for contrast in an MR image is governed by the application of an RF pulse and, more important, the relaxation times of the tissue of interest, in particular T1 and T2. After the RF pulse, an MR signal is created.

Page 26

T1 weighting of the image is dependent on the amount of TR in milliseconds between the slice selection and RF pulses and the field strength.

Page 26

T2-weighted images are dependent on the amount of TE in milliseconds.

Page 30

The real power of MR imaging lies in the wide range of applications for which it can be used. Current applications include soft-tissue delineation, determining extent of disease, tumor staging, functional and metabolic information, and monitoring response to treatment.

HOME STUDY EDUCATIONAL SEMINARS ORDER FORM

Back issues of SMRT educational seminars are for sale to SMRT members only!

Qty.	Vol.	No.	Home Studies Title
	1	1	Functional MRI: Capabilities and Limitations
	1	2	Concepts in MR Physics
	2	1	Considerations in Low Field MRI
	2	2	Directions in Basic Cardiac Imaging
	2	3	Directions in Advanced Cardiac Imaging
	2	4	The Basics of Magnetic Resonance Angiography
	3	1	Introduction to Spectroscopy
	3	2	Renal MR Imaging
	3	3	A Primer on MR Pulse Sequences
	3	4	Artifacts Encountered in Abdominal MRI
	4	1	Safety Aspects in MRI
	4	2	Directions in MRI of the Liver
	4	3	MR Techniques in the Evaluation of the Uterus
	4	4	Fundamental Principles for MR Imaging of the Brain
	5	1	Atlas of Cranial Neuroanatomy
	5	2	MRI of the Ankle & Foot
	5	3	MR Imaging of the Breast
	5	4	Diffusion-Weighted Imaging of the Brain
	6	1	Directions in MRA of the Abdominal Aorta and
	6	2	Fundamental Principles of MR Imaging of the Head,
	6	3	Advances in Interventional MRI
	6	4	Diffusion-Weighted MR Imaging of the Pediatric
	7	1	The Role of Neuroimaging in the Diagnosis of
	7	2	Cardiovascular MRI: Update I
	7	3	K-Space in the Clinic
	7	4	MR Imaging and Spectroscopy of the Prostate

Qty	Vol.	No.	Home Studies Title
	8	1	Atlas of Knee Anatomy
	8	2	Cardiovascular MRI: Update II
	8	3	Update: Safety in MR Examinations
	8	4	Parallel MR Imaging
	9	1	MRI of Breast Cancer: Update I
	9	2	MR Atlas of the Shoulder
	9	3	Exploring Magnetic Field Strengths: Challenges and
	9	4	MRI of Breast Cancer: Update II
	10	1	MR Imaging of Perfusion
	10	2	MR Imaging Artifacts:Appearance, Cause & Cure
	10	3	Techniques in Cardiovascular MR Imaging
	10	4	MRI of the Brain
	11	1	Update: Musculoskeletal MRI
	11	2	Contrast Media in MRI Examinations
	11	3	Head and Neck MRI at 3.0T
	11	4	MR Imaging of the Abdomen
	12	1	Contrast-Enhanced Musculoskeletal MR Imaging
	12	2	Neuro MRI: Principles and Protocols
	12	3	MR Imaging of the Spine
	12	4	MR Imaging of the Liver
	13	1	MR Imaging Sequences: Gradient-Recalled Echo
	13	2	Techniques in Cardiac MR Imaging
	13	3	Phase Contrast MR Imaging: Techniques and Applications
	13	4	MRI of Spinal Cord Lesions
	14	1	Breast MRI: DCIS and Skin Lesions
	14	2	Pediatric Magnetic Resonance Imaging

YOUR ORDER

Total quantity ordered: _____ x US$25 each = $_____ Subtotal* = US$_____

* PLEASE NOTE: **Your order will not include shipping.** We will contact you with the shipping cost before we process your order. No orders will be processed before you have confirmed the actual shipping cost.

PAYMENT OPTIONS & BILLING INFORMATION

PAYMENT WITHIN USA:
Personal checks, money orders, cashier's checks and company checks are acceptable. Institutional purchase orders are acceptable and will be invoiced, but payment must still be received prior to shipment.

PAYMENT FROM OUTSIDE USA:

Checks: The check must be payable "to" (NOT "through") a U.S. bank in U.S. Dollars. The check must be imprinted with the computer encoding and routing information authorized by the American Banking Association.

Traveler's Checks: Traveler's checks in U.S. dollars for the exact amount, properly counter-signed, are acceptable. International Money Order: The money order must be in U.S. dollars and be imprinted with the computer encoding and routing information authorized by the American Banking Association. U.S. dollar International Postal Money Orders imprinted as stated above are acceptable.

Wire: DO NOT PAY BY WIRE.

SMRT Member ID# (REQUIRED)_____

Name_____

Address_____

City_____State/Province_____

Postal Code/ZIP + 4_____Country_____

Phone_____Fax_____

E-mail_____

❒ Credit Card: ❒ VISA ❒ MasterCard ❒ AMEX

Credit card orders may be faxed directly to SMRT: +1 510 841 2340

Card Number: _____

Expiration Date_____Security Code_____

Billing Address_____

Billing Zip + 4/Postal Code:_____

Signature:_____

SMRT | A WORLD OF KNOWLEDGE
FOR MR TECHNOLOGISTS & RADIOGRAPHERS

SECTION FOR MAGNETIC RESONANCE TECHNOLOGISTS
OF THE INTERNATIONAL SOCIETY FOR MAGNETIC RESONANCE IN MEDICINE

Home Studies Educational Seminars are available to ISMRM members



SUBSCRIBE TODAY!

To sign up for your annual subscription, please visit:

http://www.ismrm.org/smrt/homestudy

To sign up your MR technologists to become members of the SMRT, please visit:

http://www.ismrm.org/smrt/smember2.htm

Thanks!

Anne Marie Sawyer, Editor
SMRT Educational Seminars Home Study Program

Dan Spielman, Ph.D., enjoys an SMRT Educational Seminars Home Study.

ISMRM ONE COMMUNITY FOR CLINICIANS AND SCIENTISTS

SMRT ISMRM SECTION FOR MAGNETIC RESONANCE TECHNOLOGISTS

GO TO WWW.ISMRM.ORG/SMRT OR CALL +1 510 841 1899

TO FIND OUT MORE ABOUT SMRT MEMBERSHIP, EDUCATIONAL PROGRAMS AND THE LATEST MR NEWS

NOTES

WE ARE A NETWORK OF KNOWLEDGE



SMRT – A Global Community

The Section for Magnetic Resonance Technologists (SMRT) of the International Society for Magnetic Resonance in Medicine (ISMRM) is the leading non-profit organization that provides an international forum for education, information and research in magnetic resonance for technologists and radiographers throughout the world.

The SMRT was established by technologists, clinicians and scientists of the ISMRM as a forum for technologists and radiographers to share their expertise and educational resources, with a common goal of improving healthcare for people worldwide.

As an organization, we are committed to promoting communication and the dissemination of cutting-edge MR developments. The objective of the SMRT is to advance education and training, while striving to promote a high level of knowledge and professionalism in the field of MR technology and radiography.

SMRT

ISMRM

SECTION FOR MAGNETIC RESONANCE TECHNOLOGISTS

2030 ADDISON STREET • SUITE 700
BERKELEY, CALIFORNIA, 94704 USA
TEL: +1 510 841 1899
FAX: +1 510 841 2340
INFO@ISMRM.ORG/SMRT